



**HAL**  
open science

# Prediction of Flexible Pipe Annulus Composition by Numerical Modeling: Identification of Key Parameters

Xavier Lefebvre, Nina Khvoenkova, Jean-Charles de Hemptinne, Léa Lefrançois, Béatrice Radenac, Stéphanie Pignoc-Chicheportiche, Cécile Plennevaux

## ► To cite this version:

Xavier Lefebvre, Nina Khvoenkova, Jean-Charles de Hemptinne, Léa Lefrançois, Béatrice Radenac, et al.. Prediction of Flexible Pipe Annulus Composition by Numerical Modeling: Identification of Key Parameters. *Science and Technology for Energy Transition*, 2022, 77, pp.11. hal-03695308

**HAL Id: hal-03695308**

**<https://ifp.hal.science/hal-03695308>**

Submitted on 14 Jun 2022

**HAL** is a multi-disciplinary open access archive for the deposit and dissemination of scientific research documents, whether they are published or not. The documents may come from teaching and research institutions in France or abroad, or from public or private research centers.

L'archive ouverte pluridisciplinaire **HAL**, est destinée au dépôt et à la diffusion de documents scientifiques de niveau recherche, publiés ou non, émanant des établissements d'enseignement et de recherche français ou étrangers, des laboratoires publics ou privés.



Distributed under a Creative Commons Attribution 4.0 International License

# Prediction of flexible pipe annulus composition by numerical modeling: identification of key parameters

Xavier Lefebvre<sup>1,\*</sup>, Nina Khvoenkova<sup>1</sup>, Jean-Charles de Hemptinne<sup>1</sup>, Léa Lefrançois<sup>2</sup>, Béatrice Radenac<sup>2</sup>, Stéphanie Pignoc-Chicheportiche<sup>2</sup>, and Cécile Plennevaux<sup>2</sup>

<sup>1</sup>IFP Energies nouvelles, 1 et 4 avenue de Bois-Préau, 92852 Rueil-Malmaison, France

<sup>2</sup>Flexi France, TechnipFMC, Rue Jean Huré, 76580 Le Trait, France

Received: 29 October 2021 / Accepted: 30 March 2022

**Abstract.** This article describes recent improvements made in the design process of offshore flexible pipes. These improvements consider the more precise complex geometry and architecture of the flexible pipes, while considering their corrosive environment (high pressure, high temperature, acid gases (CO<sub>2</sub>, H<sub>2</sub>S), sea water, etc.) and the relevant physics. MOLDI<sup>TM</sup>, the design software that was developed 20 years ago to predict flexible pipes annulus environment, has been constantly upgraded to increase its representativeness: use of chemical potential or fugacity to better describe the mass transport, improvement of the thermodynamic module to better describe the interaction between chemical species and allow to model the purging through gas release valves. Recently, a major advance has been made allowing to cope with flooded annulus flexible pipes. When the annulus is flooded, the tortuosity produced by the presence of steel wires inside the annulus can take a major importance. Therefore, a new model, named 3DIFF, has been developed to describe the 3-dimensional characteristics of the annulus and its impact on fugacity profile across the structure. Depending on permeation properties of each layer, the result is that the presence of water can produce a fugacity gradient within the annulus. This heterogeneity must be considered during the design process to be fully representative of service conditions and allow to select flexible pipes materials with confidence. Experimental devices used to generate permeation database are under constant evolution to study even more complex mechanisms such as the diffusion process in a flooded tortuosity or the compression effects of polymeric material on their permeation properties.

**Keywords:** Diffusion, Thermodynamics, Modeling, Flexible Pipe, Design, Corrosion, Carbon dioxide, MOLDI, 3DIFF.

## Nomenclature

$J_i$	Flux of compound $i$ (mol m <sup>-2</sup> s <sup>-1</sup> )	$Z$	Compressibility factor
$\mathcal{D}_i$	Fick's diffusion coefficient (m <sup>2</sup> s <sup>-1</sup> )	$k_{ij}$	Binary interaction parameter between $i$ and $j$
$c_i$	Concentration of compound $i$ (mol m <sup>-3</sup> )	$\beta_{ij}$	Parameter which describes the volume between $i$ and $j$
$C$	Global concentration (mol m <sup>-3</sup> )	$\varepsilon_{ij}$	Parameter which describes the energy of association between $i$ and $j$
$x_i$	Mole fraction of compound $i$	$T_c$	Critical temperature (K)
$n_i$	Number of moles of component $i$ (mol)	$P_c$	Critical pressure (Pa)
$\mu_i$	Chemical potential of compound $i$ (J mol <sup>-1</sup> )	$D_0$	Pre-exponential factor for the diffusion coefficient in polymers (m <sup>2</sup> s <sup>-1</sup> )
$D_i$	Thermodynamic diffusion coefficient (m <sup>2</sup> s <sup>-1</sup> )	$S_0$	Pre-exponential factor for the solubility coefficient in polymers (mol m <sup>-3</sup> bar <sup>-1</sup> )
$R$	Perfect gas constant (8.314 J mol <sup>-1</sup> K <sup>-1</sup> )	$E_D$	Activation energy for the diffusion coefficient in polymers (J mol <sup>-1</sup> )
$T$	Temperature (K)	$E_S$	Activation energy for the solubility coefficient in polymers (J mol <sup>-1</sup> )
$a_i$	Activity of the diffusing compound $i$	$w$	Real width of the helix (m)
$f_i$	Fugacity of the compound $i$ (bar)		
$S_i$	Solubility coefficient of compound $i$ (mol m <sup>-3</sup> bar <sup>-1</sup> )		

\* Corresponding author: [xavier.lefebvre@ifpen.fr](mailto:xavier.lefebvre@ifpen.fr)

$w'$	Width of the equivalent layer in the 2D axisymmetric model (m)
$a$	Laying angle (rad)
$P'$	Pitch of the helix (m)
$R'$	Radius of the helix (m)
$R_{\text{MEAN}}$	Average radius (m)
$R_{\text{INT}}$	Internal radius (m)
$e$	Thickness of the layer (m)
$f$	Gap between two rings in the 2D axisymmetric model (m)
$z$	Position along the pipe axis (m)
$P_{\text{vent}}$	Venting pressure (bar)
$P_{\text{annulus}}$	Annulus pressure (bar)
$P_{\text{vent\_closure}}$	Pressure at which the valve turns close (bar)
$V$	Total volume (m <sup>3</sup> )
$v$	Molar volume (m <sup>3</sup> mol <sup>-1</sup> )
$v_{\text{light}}$	Volume of the light phase (m <sup>3</sup> )
$v_{\text{heavy}}$	Volume of the heavy phase (m <sup>3</sup> )

## 1 Introduction

Flexible pipes are used for transporting fluids over long distances, often subsea. They have many advantages [1], but require a careful design in order to provide mechanical strength, corrosion resistance and impermeability towards the fluids that are thus transported [2]. This is why they are constructed out of several metallic and polymeric layers. The purpose of this paper is to discuss two pieces of software that have been developed in a collaboration between *TechnipFMC* and *IFPEN* with the objective to model the radial permeation phenomena that occur within these pipes.

Polymer sheaths are permeable to some chemical compounds carried by flexible pipes. As a consequence, in operation, a corrosive environment may be established in the annulus, between the internal and the external sheaths. The performance of structural steel wires is strongly linked to the properties of the annulus medium which can be predicted by modeling. *MOLDI*<sup>TM</sup> is the design software that has been developed 20 years ago to predict flexible pipes annulus environment [3]. Among its options, this software enables to predict the condensation of water, the purging by gas release valves and to calculate the fugacity of the different gases along time up to the equilibrium. The fugacity of acid gases (CO<sub>2</sub> and H<sub>2</sub>S) has a major impact on the materials selection which is one of the most important step in the design of flexible pipes.

The modeling process has been revisited and major improvements have been made. The objective of this paper is to present the theoretical basis of the diffusion process modeling and the thermodynamic module. The development of a new model, called 3DIFF, representative of the flexible pipe geometry is also detailed. Finally, part of the data related to the validation of the calculations is presented and then a discussion about the application area of the models is proposed. The advantages of both models will be also discussed.

## 2 Background and nomenclature

The flexible pipe is a complex three-dimensional structure typically made of polymer and metallic layers. The illustration of a structure with insulation option is presented in [Figure 1](#) highlighting the following layers (from inside to outside of the structure):

- A carcass, which is a metallic construction used to prevent collapse of the pipe or the internal pressure sheath due to external pressure for example, or crushing loads.
- An internal pressure sheath, which is an extruded polymer layer that ensures internal fluid containment.
- A pressure vault, which is a structural layer with a laying angle close to 90°, to increase the resistance of the pipe to internal and external pressure. This layer is typically made of interlocked shaped carbon steel wires and may be reinforced by an additional layer of flat wires, laid at opposite angle.
- Tensile armor layers, which are structural layers with a laying angle typically between 20° and 55°, and consist of helically wounded wires. They are used to sustain tensile loads and internal pressure. Tensile armor layers are carbon steel flat wires and are counter-wounded in pairs.
- Anti-wear layers, which are non-metallic extruded thermoplastic tape wrappings, used to avoid wear between structural layers.
- An outer sheath, which is an extruded polymer layer that protects the pipe against penetration of seawater and external damages.
- Insulation layers may be added for flow assurance purpose to increase the pipe thermal insulation properties and to prevent hydrate formation. Typically, the insulation tapes are wounded on top of an intermediate sheath or directly on top of the tensile armors and are protected by the external sheath. The insulation annulus is often free flooded with sea water during flexible pipe installation.

In operation, when flexible pipes carry the fluid, chemical species like CO<sub>2</sub>, CH<sub>4</sub>, H<sub>2</sub>S and water diffuse through polymer sheaths until an equilibrium is reached in the annulus. To assess the properties of the fluid in contact with the steel wires and polymers in the annulus, different processes are taken into account:

- The diffusion of species as a function of the temperature gradient, the inner and outer pressures and the fugacities gradients.
- The phase changes within the annular space.
- The corrosion of wires and the high confinement in the annulus (low volume over steel surface ratio) leading to a supersaturation with corrosion products. This supersaturation mainly affects the H<sub>2</sub>S content in the annulus, as it is highlighted experimentally, due to the slow inlet of H<sub>2</sub>S and its consumption.

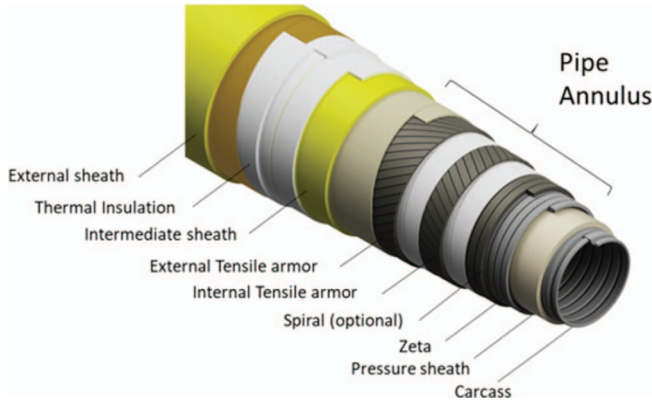


Fig. 1. Typical flexible pipe structure with insulation option.

MOLDI<sup>TM</sup> is the software developed by *IFPen* and *TechnipFMC* to predict the annulus environment. A first technical paper about this model was published 20 years ago [3]. The objective of this new paper is to present the improvements over the last years:

- The diffusion process is better described using updated physical equations, taking into account the complex geometry of the diffusion path and the impact of water in the annuli when flooded.
- The thermodynamic model has been improved.
- The permeability database is continuously maintained and improved in line with the new data available.

The methodology used to get the equivalent H<sub>2</sub>S partial pressure taking into account its consumption has been published before [4–8] and will not be presented in this paper.

### 3 Physical principles and governing equations

#### 3.1 Mass transport

The diffusion in polymer systems is often described using Fick's law (1). This was also the starting point in our earlier work [3]:

$$J_i|_{T,P} = -\mathfrak{D}_i \cdot \nabla c_i, \quad (1)$$

where  $J_i$  is the flux (in mol m<sup>-2</sup> s<sup>-1</sup>) and  $c_i$  the species concentration (in mol m<sup>-3</sup>). Fick's diffusion coefficient  $\mathfrak{D}_i$  is a proportionality factor (in m<sup>2</sup> s<sup>-1</sup>). The same equation can also be written as:

$$J_i|_{T,P} = -\mathfrak{D}_i \cdot C \nabla x_i, \quad (2)$$

where  $x_i$  is the mole fraction and  $C$  is now the global concentration in mol m<sup>-3</sup>.

Fick's law implies a number of assumptions, as for example that the compounds (solvent + solute(s)) mixture behave as in an "ideal mixture" which means that they have no interactions with one another, or there is no flux coupling. It also assumes that the diffusion coefficient is inde-

pendent of the operating conditions (it only depends on temperature). As discussed by several authors [9–11], and based on Stefan-Maxwell theory, it is however demonstrated that the true driving force for diffusion is in fact the chemical potential. In isothermal and isobaric conditions, the diffusion law should therefore be stated as:

$$J_i|_{T,P} = -c_i \cdot D_i \cdot \frac{\nabla \mu_i}{RT}, \quad (3)$$

where  $D_i$  is called the thermodynamic diffusion coefficient. The molar concentration of compound  $i$  remains outside the gradient, because the flux is proportional to the concentration. Equation (3) is sometimes written as

$$J_i|_{T,P} = -C \cdot D_i \frac{\partial \ln a_i}{\partial \ln x_i} \Big|_{T,P} \cdot \nabla x_i, \quad (4)$$

where  $a_i$  is the activity of the diffusing compound  $i$  and the derivative  $\frac{\partial \ln a_i}{\partial \ln x_i} \Big|_{T,P}$  is called the thermodynamic factor. These expressions lead to the following relationship between the Fick and the thermodynamic diffusion coefficient:

$$\mathfrak{D}_i = D_i \frac{\partial \ln a_i}{\partial \ln x_i} \Big|_{T,P}. \quad (5)$$

A thermodynamic model is required to compute the thermodynamic factor.

In this work, an alternative is proposed. The chemical potential is related to the fugacity of a component in a mixture as

$$\mu_i = \mu_i^\#(T, P_0) + RT \ln \frac{f_i}{f_i^\#(T, P_0)}, \quad (6)$$

where the hash sign (#) refers to a reference state that may be taken as the same mixture in the ideal gas state (in which case the fugacity ratio becomes a fugacity coefficient that is computed from an equation of state), or as the pure component  $i$  in the same physical state as the mixture (in which case the fugacity ratio is the activity that was encountered in Eq. (4)). Considering that here only the gradient is looked at, the choice of reference state does not matter and we have:

$$\nabla \mu_i|_{T,P} = RT \nabla \ln f_i|_{T,P} = \frac{RT}{f_i} \nabla f_i|_{T,P}. \quad (7)$$

Combining equation (7) with equation (3) now yields:

$$J_i|_{T,P} = -\frac{c_i \mathfrak{D}_i}{f_i} \nabla f_i \Big|_{T,P} = -S_i \mathfrak{D}_i \nabla (f_i), \quad (8)$$

where

$$S_i = \frac{c_i}{f_i} \quad (9)$$

is the solubility coefficient. As a first approximation, the fugacity behaves linearly with the concentration. Hence, we shall consider this ratio to be a constant (only depend-

ing on temperature). This is not exactly true, because of the large size difference between solute and solvent (polymer). This is why, as will be discussed later, the value is updated at every time step.

From the mass balance, the concentration increase in each point is then expressed as:

$$\left. \frac{\partial c_i}{\partial t} \right|_{T,P} = -\nabla(J_i) = \nabla(S_i D_i \nabla(f_i)). \quad (10)$$

And, because of equation (9):

$$\left. \frac{\partial(S_i f_i)}{\partial t} \right|_{T,P} = \nabla(S_i D_i \nabla(f_i)). \quad (11)$$

We further consider that  $S_i$  is independent of time. In fact,  $S_i$  depends on composition, which changes with time, so that it is indirectly dependent on that property. We then find:

$$S_i \left. \frac{\partial(f_i)}{\partial t} \right| = \nabla \cdot (S_i D_i \nabla(f_i)). \quad (12)$$

The diffusion law is then written with the fugacity coefficient and involves the diffusion and solubility coefficients.

On discontinuities, *i.e.* between the materials, the following conditions apply:

- Continuity of fugacity flux of  $q_f$ :

$$q_f = -D_i^- S_i^- (n \cdot \nabla f^-) = -D_i^+ S_i^+ (n \cdot \nabla f^+). \quad (13)$$

- Continuity of fugacity:

$$f^+ = f^-. \quad (14)$$

When the problem is composed of several  $n_f$  components, the mass transport problem is treated independently for each component. The result of this calculation is the determination of the fugacity,  $f_i$ , for each component  $i$  and each time step.

### 3.2 Physical parameters in the polymer

Both solubility coefficient (defined in (9)) and diffusion coefficient (defined in (3)) within the polymer are expressed using an Arrhenius law:

$$D_i = D_{i,0} \exp\left(-\frac{E_{i,D}}{RT}\right) \quad (15)$$

and

$$S_i = S_{i,0} \exp\left(-\frac{E_{i,S}}{RT}\right), \quad (16)$$

where  $R$  is the ideal gas constant;  $D_{i,0}$  and  $S_{i,0}$  are the pre-exponential factor and  $E_{i,D}$ ,  $E_{i,S}$  the activation energies for respectively  $D$  and  $S$ .

For each polymer/gas pair,  $D_{i,0}$ ,  $S_{i,0}$ ,  $E_{i,D}$ ,  $E_{i,S}$  are determined experimentally [12]. For all polymeric materials that are used in the flexible pipes, permeation tests are performed with  $\text{CO}_2$ ,  $\text{CH}_4$  and  $\text{H}_2\text{S}$ , either as pure gas or as gas mixture for specific purposes. Inside a representative temperature range, the experiments are performed at three constant temperatures at least in order to determine the Arrhenius coefficients for each polymer/gas pair. Standard permeation tests are typically performed in a two compartments isothermal cell as illustrated in Figure 2: one gas charging cell and one gas collection cell separated by a polymer plane membrane. The quantification of species in the permeation flowrate is made by gas chromatography.

Besides experiments, some work is in progress in order to use SAFT (Statistical Associating Fluid Theory) [13] and PC-SAFT (Perturbed-Chain SAFT) [14] equation of states to calculate the solubility of gases inside the polymer. This approach has been successfully used in [15]. In particular, the swelling of the polymer may be considered since its mechanical confinement might lower the solubility and probably also the permeability.

### 3.3 Thermodynamic description of the annular space

As shown in equation (14), the fugacity in the annular space is taken equal to that in the polymer. Equation (13) implies that a fugacity gradient also exists in this empty space, except if a large value is taken for the diffusion coefficient. This is the hypothesis that is made when the free space is dry; the fugacity is thus considered to be a constant throughout the annulus.

The material that accumulates in this space will, however, increase the local pressure, and possibly condensation will occur. In order to model this, an Equation of State (EoS) is coupled to a flash algorithm so as to make it possible to compute pressure at fixed temperature and volume (the volume of the annulus), or to compute the volume as a function of pressure and temperature. These calculations are further referred to as “TV flash” and “TP flash”. They allow computing the phase equilibrium as well as the fugacities of all components when the composition of the annulus is known. The way diffusion and flash calculations are coupled is further detailed in Section 4.3.

#### 3.3.1 The CPA equation of state

Considering the composition, pressure and temperature range of this work the Cubic Plus Association (CPA) equation of state is selected. It is constructed as a combination of a cubic Equation of State (EoS) and an associative term, proposed by Kontogeorgis *et al.* [16]. The compressibility factor  $Z$  is expressed using the equation:

$$Z = \frac{1}{1-\eta} - \frac{(a/bRT)\eta}{1+\eta} + \sum_i x_i \sum_j \rho_j \sum_{A_j} \left[ \left( \frac{1}{X^{A_j}} - \frac{1}{2} \right) \frac{\partial X^A}{\partial \rho_i} \right] \quad (17)$$

where  $\eta = b/v$  and  $\rho_i = n_i/v$ . The first two terms come from the Soave-Redlich-Kwong (SRK) cubic equation

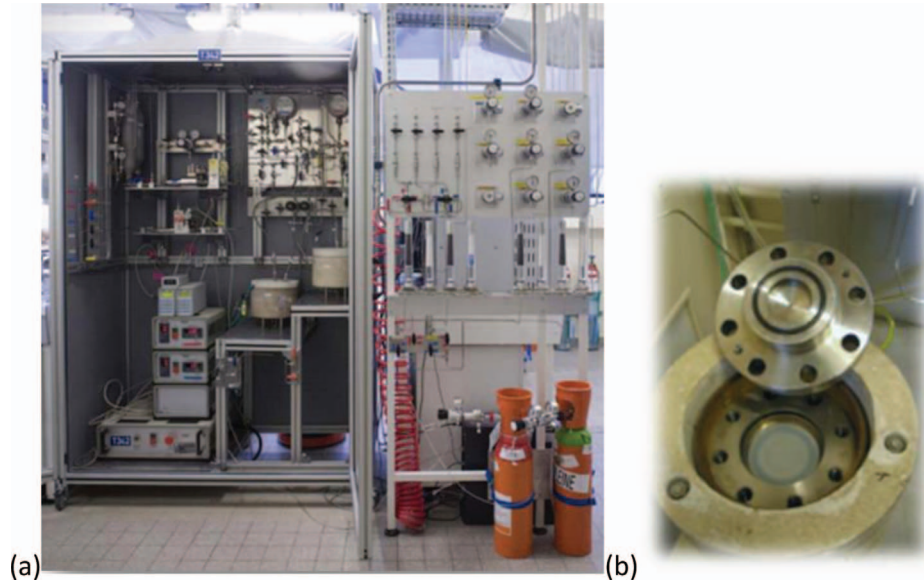


**Fig. 2.** Picture of a two compartments permeability unit (a) and picture of a polymer membrane placed at the interface of the two compartments (b).

and the last comes from Wertheim's theory. This term, called "associative", allows to take into account that some molecules form dimers, or even multi-mers when they are sufficiently close to each other. These interactions are described using pseudo-chemical equilibrium, assigning each species a number of electropositive and electronegative sites. Thus, while preserving the cubic characteristics for non-associative molecules such as hydrocarbons, CPA significantly improves the predictive power of the EoS, especially for mixtures containing species such as ethanol, methanol or water.

In this version of CPA, the  $a_i$  parameters depend on temperature (careful, the symbol here is different from the activity that was shown in equations (4) and (5)):

$$a_i(T) = a_{c,i} \left[ 1 + c_i \cdot \left( 1 - \sqrt{T/T_{c,i}} \right) \right]^2. \quad (18)$$

The parameters  $a_{c,i}$ ,  $b_i$  and  $c_i$  are provided directly. In mixtures, they are subject to mixing rules: ( $x_i$  is the mole fraction of component  $i$ ):

$$b = \sum_i x_i b_i \quad (19)$$

and

$$a = \sum_i \sum_j x_i x_j \sqrt{a_i a_j} (1 - k_{ij}), \quad (20)$$

where the parameter  $k_{ij}$  (default null) allows to correct the classic mixing rule for a specific binary. This parameter may be a function of temperature:

$$k_{ij} = k_{ij}^{(0)} + k_{ij}^{(1)} T + k_{ij}^{(2)} T^2. \quad (21)$$

In the associative term of equation (17), we see the variables  $X^{A_i} = n^{A_i}/n_i$  that describe the unbound fraction of site  $A$

on molecule  $i$ . These unbound fractions are themselves derived from solving the following equation for each of the sites in the system:

$$X^{A_i} \left[ 1 + \sum_j \sum_B \left( \frac{n_j}{V} X^{B_j} \Delta^{A_i B_j} \right) \right] = 1. \quad (22)$$

It shows the strength of association between two sites, which is calculated as follows:

$$\Delta^{A_i B_j} = g(v) b_{ij} \beta_{ij} \left[ \exp \left( \frac{\varepsilon_{ij}}{kT} \right) - 1 \right], \quad (23)$$

where  $g(v)$  is the radial distribution function, computed as:

$$g(v) = \frac{1}{1 - 1.9 \frac{v}{4v}}. \quad (24)$$

The parameters  $\beta_{ij}$  and  $\varepsilon_{ij}$  are new parameters, which describe the volume and the energy of association between the two species  $i$  and  $j$ , respectively.

In a mixture, the parameters  $\beta_{ij}$  and  $\varepsilon_{ij}$  are calculated from the pure compound ones using following combining rules:

$$\varepsilon_{ij} = (1 - w_{ij}) \frac{\varepsilon_i + \varepsilon_j}{2} \quad (25)$$

and

$$\beta_{ij} = (1 - u_{ij}) \sqrt{\beta_i \beta_j}, \quad (26)$$

$\varepsilon_i$  and  $\beta_i$  are specific to each associative compound. It should be mentioned that the associative term deals with auto-associative bodies but that it is also possible to consider cross associations even in the presence of a non-associative molecule (*e.g.*, CO<sub>2</sub>).

**Table 1.** CPA pure component properties (more details in [3]).

Component	$a_{c,i}$ (Pa m <sup>3</sup> /mol)	$b_i$ (m <sup>3</sup> /mol)	$c_i$ (-)	$N_{\text{sites}}$ (*)	Charges (**)	$\varepsilon_i/k$ (K)	$\beta_i$
H <sub>2</sub> O	0.12274	1.45E-05	0.67359	4	++-	2002.7	0.0692
H <sub>2</sub> S	0.44505	2.85E-05	0.60265	2	-	500	0.05
CO <sub>2</sub>	0.35080	2.72E-05	0.76020	1	-	1413.0	0.0037924
CH <sub>4</sub>	0.23204	2.91E-05	0.44718	0	0	0	0

\* $N_{\text{sites}}$  is the number of sites on the molecule.

\*\*This shows the association scheme, *i.e.* the sign of the charges on each site.

**Table 2.** Binary parameters for CPA. In the table,  $w_{ij}$  is the parameter from equation (25),  $u_{ij}$  from equation (26) and  $k_{ij}$  is a polynome as expressed in equation (21).

H <sub>2</sub> O–H <sub>2</sub> S	This work
$w_{ij}$	-0.04551175
$u_{ij}$	-0.06083181
$k_{ij}^{(0)}$	0.191
H <sub>2</sub> O–CO <sub>2</sub>	This work
$k_{ij}^{(0)}$	0.1141
H <sub>2</sub> O–CH <sub>4</sub>	This work
$k_{ij}^{(0)}$	-1.41407
$k_{ij}^{(1)}$	0.00668657
$k_{ij}^{(2)}$	-6.52698E-006
CO <sub>2</sub> –H <sub>2</sub> S	This work
$k_{ij}^{(0)}$	0.0519
CO <sub>2</sub> –CH <sub>4</sub>	[19]
$k_{ij}^{(0)}$	0.08818

### 3.3.2 Parameters

In this work, we consider four possible diffusing species: H<sub>2</sub>O, H<sub>2</sub>S, CO<sub>2</sub> and CH<sub>4</sub>.

The CPA EoS requires three to five parameters (five parameters in the case of water, which is an associating compound) for each compound. The mixtures investigated in this work have been previously discussed by Ruffine *et al.* [17, 18] and Tsvintzelis *et al.* [19] and we have taken their parameters. Often, Ruffine uses temperature-dependent interaction parameters, while Tsvintzelis uses constant parameters. In this work, a selection is made. Table 1 provides the pure component parameters.

The final binary interaction parameters are given in Table 2. Note that all parameters are symmetric ( $ij = ji$ ). They generally come from literature, except for water–methane that have been further improved in this work using a quadratic  $k_{ij}$  function.

### 3.3.3 Validation

The equation of state is validated on all binary systems that are considered in this work. The graphs in Figures 3 and 4 are examples of the model results.

The water + CO<sub>2</sub> system is probably one of the most difficult one to represent correctly because the CO<sub>2</sub> critical point is located within the domain of interest. Both figures show how the mutual solubility curves change from 25 °C (subcritical: at low pressure, there is a clear change in behaviour between vapor CO<sub>2</sub>, below 5 MPa, and liquid CO<sub>2</sub>, above 5 MPa) to 100 °C where the solubility lines become smooth. The higher deviation observed at high pressure in Figure 4 is a drawback of the model: a compromise had to be found so that the deviation remains reasonable throughout the domain of interest.

Figure 5 shows the same information for the binary system methane + water. This behaviour is smooth throughout the region of interest, and the model represents the experimental behaviour rather well.

## 4 Simplified 2D diffusion model coupled with a thermodynamic module (MOLDI™)

### 4.1 Description of MOLDI™ 2D geometry

In order to get an efficient engineering tool, a 2D simplified axisymmetric geometry is considered in the model for mass diffusion. The flexible pipe layers can be defined in two categories: continuous layers (thermoplastic cylindrical sheathes) and discontinuous layers (steel wires, anti-wear tapes, holed anti-wear sheath, thermal insulation foams, etc.). An annulus is defined as the space between two continuous layers.

For the continuous layers, the transposition from the complete 3D structure to the 2D axisymmetric geometry is obvious. There is no change in the radial dimensions (internal radius and thickness).

The shielding effect is a phenomenon induced by the direct contact of a continuous polymer layer and a discontinuous steel layer. Indeed, the steel component of the discontinuous layer will act as a barrier to the fluid permeating through the continuous polymer layer. Only a portion of the outer interface of the polymer sheath will allow the fluid to permeate. The size of this portion is directly related to the gap between steel wires. Consequently, the shielding effect induces an overall reduction of the quantity of fluid permeating through the sheath. Experimentally, this effect has been validated using small scale, middle scale and full scale permeation tests. This phenomenon is illustrated in Figure 6. By construction, the shielding effect is taken into account in the simplified 2D

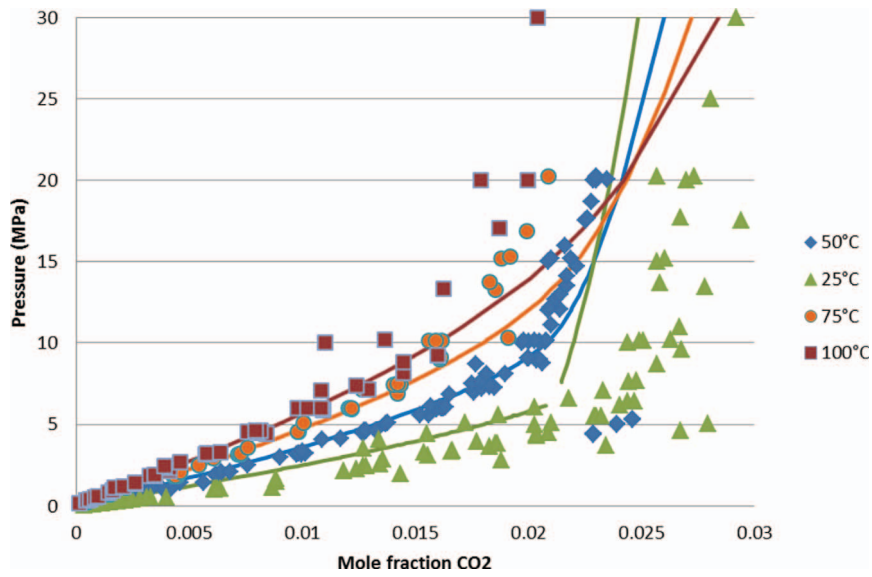


Fig. 3. Solubility of CO<sub>2</sub> in water. Data (points) are taken from [20–28] and curves are CPA results.

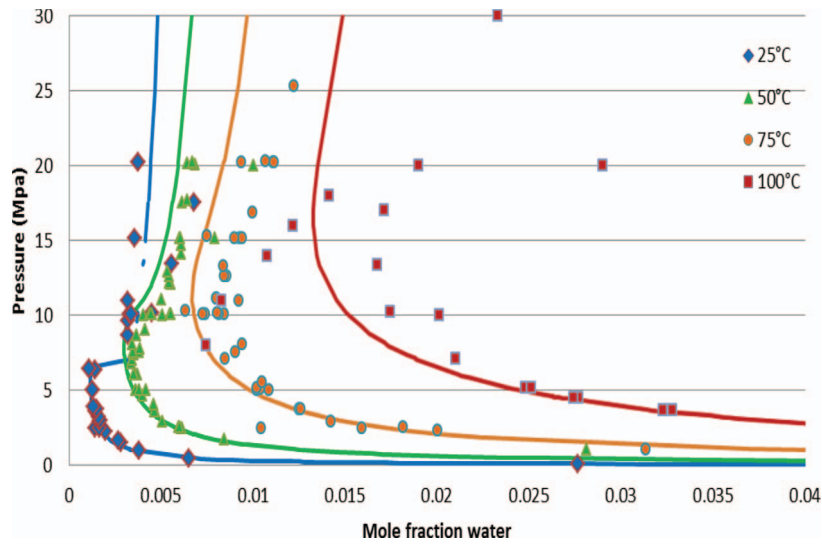


Fig. 4. Solubility of water in CO<sub>2</sub>. Data (points) are taken from [20–28] and curves are CPA results.

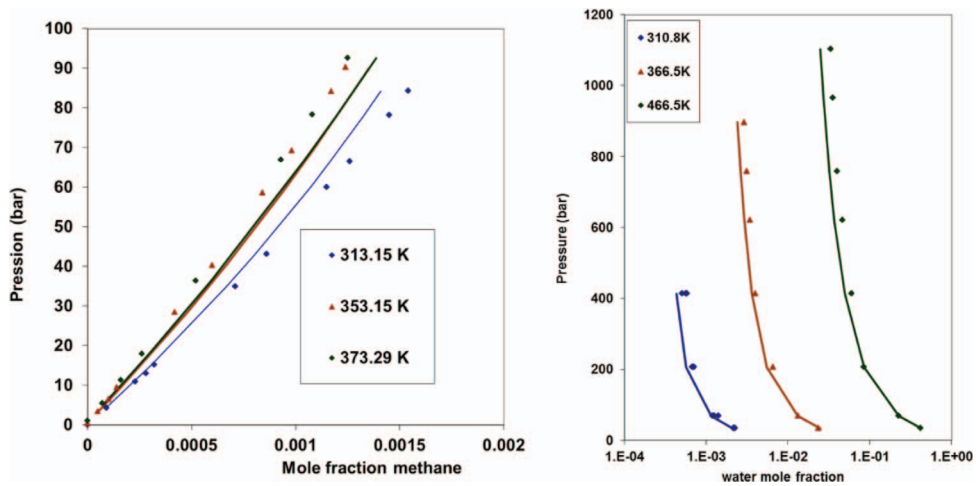
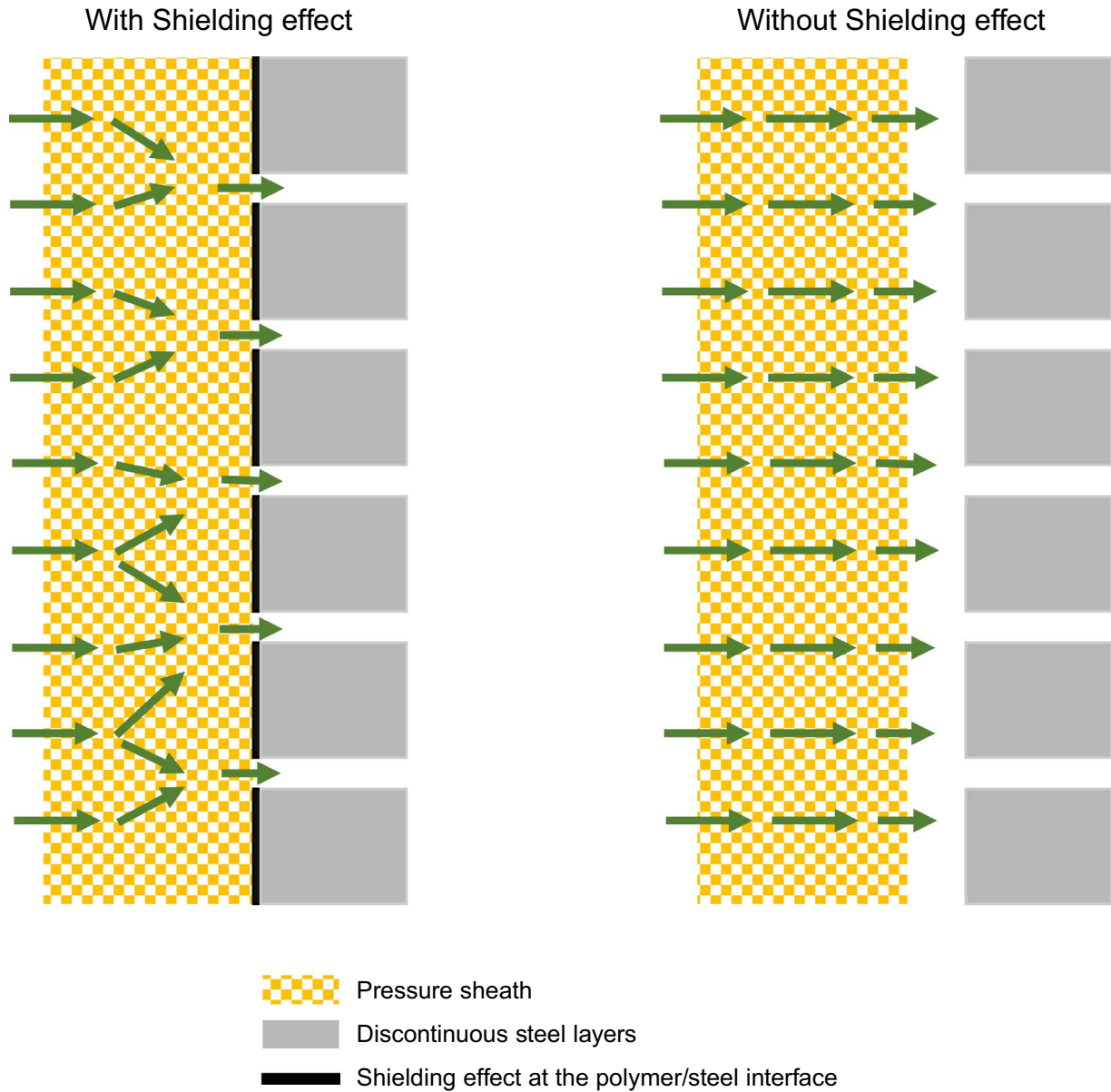


Fig. 5. Mutual solubility between methane and water. Data (points) are taken from [29] and curves are CPA results.



**Fig. 6.** Illustration of the shielding effect of a discontinuous layer on a sheath.

model according to the operating conditions of the flexible pipe.

Based on the hypothesis that the establishment of the environmental conditions in the annuli in steady state depends on:

- i) thermal, geometrical and permeation properties of the continuous layers,
- ii) the shielding effect induced by the upper discontinuous layers in contact with the continuous layers,

a simplified 2D model is created in which the annulus is represented by an equivalent layer. A schematic explanation of this simplification is presented in [Figure 7](#). This simplification is valid as long as fugacities in the annulus are homogeneous.

Helical metallic discontinuous layers are transformed as rings in the 2D axisymmetric geometry. The parameters of the helix and the parameters of the wire (laid as an helix) are illustrated in [Figure 8](#).

The pitch of the helix  $P'$  is calculated from the helix radius  $R'$  and the laying angle  $\alpha$  with the following equation:

$$P' = 2\Pi \frac{R'}{\tan(\alpha)}. \quad (27)$$

The radius of the helix for a layer of the flexible pipe is the mean radius:

$$R_{MEAN} = R_{INT} + \frac{e}{2}. \quad (28)$$

with  $R_{\text{INT}}$  the internal radius and  $e$  the thickness of the wire.

The width of the wires in the 2D axisymmetric model  $w'$  is defined as a function of the laying angle, the actual width of the wire  $w$  and the thickness of the wire  $e$ :

$$w' = \frac{w}{\sin(\alpha)}. \quad (29)$$

The equivalent gap  $j'$  between two rings in the 2D model is then calculated from:

$$j' = \frac{p'}{n} - w', \quad (30)$$

where  $n$  is the number of wires that compose the layer.

## 4.2 Physical parameters in insulation annulus

Insulation foams are discontinuous layers that are laid as helices on the flexible pipe, typically between an intermediate and an external sheath. The design of the flexible pipes is often performed considering that the insulation annulus can be flooded by seawater. The presence of water in the insulation annulus slows down the diffusion of acid gases to the external sheath and thus increases the severity of the steel wires annulus. In MOLDI<sup>TM</sup>, the insulation annulus is treated as a specific layer with equivalent permeability parameters for gases diffusion that were defined using the 3D model 3DIFF which is described in Section 5.

## 4.3 Coupling between mass transport and thermodynamic equilibrium calculations

We have seen that at the boundary between two different diffusion layers, we need to set equality of fugacities (Eq. (14)). At any given time step, the diffusion problem is first solved on the complete geometry, which provides a fugacity value,  $f_{i,t}^{\text{diff}}$  for each component at all locations, including in the annulus.

Next, the number of moles of each component  $i$  in each annulus is calculated as

$$n_{i,t} = S_{i,t-1}^a \int_{i,t}^{\text{diff}} V_{\text{annulus}}, \quad (31)$$

where  $V_{\text{annulus}}$  is the given annular volume,  $S_{i,t-1}^a$  is the solubility in the annular space. This solubility, defined as in equation (9), changes with time, as the annular space fills. This is why the subscript “ $t - 1$ ” indicates that the value is taken from the previous time step.

Once the number of moles is known, with temperature (given) and volume ( $V_{\text{annulus}}$ ), a TV flash is performed with the CPA EoS so as to determine the pressure, the phase behavior (it may be that some condensation occurs), and the fugacity, now called  $f_{i,t}^{\text{flash}}$ . If the time step is small enough, the fugacity should not be very different from the fugacity obtained from the diffusion step:

$$f_{i,t}^{\text{diff}} \approx f_{i,t}^{\text{flash}}. \quad (32)$$

Yet, when the two are different, it is possible to update the solubility as follows:

$$S_{i,t}^a = \frac{n_{i,t}}{f_{i,t}^{\text{flash}} \cdot V_{\text{annulus}}}. \quad (33)$$

Note that for the first time step, the annular space is considered to be at room pressure, so that the ideal gas law can be applied, meaning:

$$S_{i,0}^a = \frac{1}{RT}. \quad (34)$$

## 4.4 Annulus venting

The annulus, closed by default, can be vented if the annulus pressure  $P_{\text{annulus}}$  (resulting from a TV flash) is greater than the venting pressure  $P_{\text{vent}}$ . Components mole numbers  $n_{i,t}$  ( $i = 1$  to  $n_f$ ) are modified to obtain an equilibrium at the venting closure pressure  $P_{\text{vent\_closure}} = P_{\text{vent}} - \Delta P$  and the annulus free volume  $V_{\text{annulus}} \cdot P_{\text{vent}}$  and  $\Delta P$  are defined by the user as problem inputs ( $\Delta P$  is the valve opening differential pressure).

A flash calculation is then performed with temperature  $T_{\text{annulus}}$ , pressure  $P_{\text{vent\_closure}}$ , and mole numbers  $n_{i,t}$  (“TP” flash). It gives a new volume  $V$  that is larger than that of the annulus. It may be composed of one or two distinct phases (aqueous liquid and gas). Venting consists in removing the surplus material. For each component following operation is performed, before equation (33) is applied:

$$n_{i,t}^{\text{new}} = n_{i,t} - n_{i,t}^{\text{vent}}. \quad (35)$$

The phases are ordered from the lightest (usually vapor) to the heaviest (usually aqueous) based on their density, which is their molar mass divided by their molar volume (provided by the thermodynamic flash). The venting occurs always such that the lightest phase is removed first.

In the current version of MOLDI<sup>TM</sup>, venting is available in presence of two different fluid phases. The description of venting differs regarding the number of phases in presence. We may consider three cases, as shown in Figure 9.

The upper case  $V$  is the total volume, lower case is the molar volume, such that the ratio  $\frac{V}{v} = n$  expresses a mole number. The index  $i$  stands for the component of interest.

In case 1, there is only a single phase and in case 2, there are two phases, and the volume of the light phase is larger than the difference  $V - V_{\text{annulus}}$ . In these cases, we have

$$n_{i,t}^{\text{vent}} = \frac{(V - V_{\text{annulus}})}{v_{\text{light}}} x_i^{\text{light}}, \quad (36)$$

where  $v_{\text{light}}$  is the molar volume and  $x_i^{\text{light}}$  the mole fraction of  $i$  for the light phase. As a consequence,  $\frac{(V - V_{\text{annulus}})}{v_{\text{light}}}$  is the number of moles to be vented.

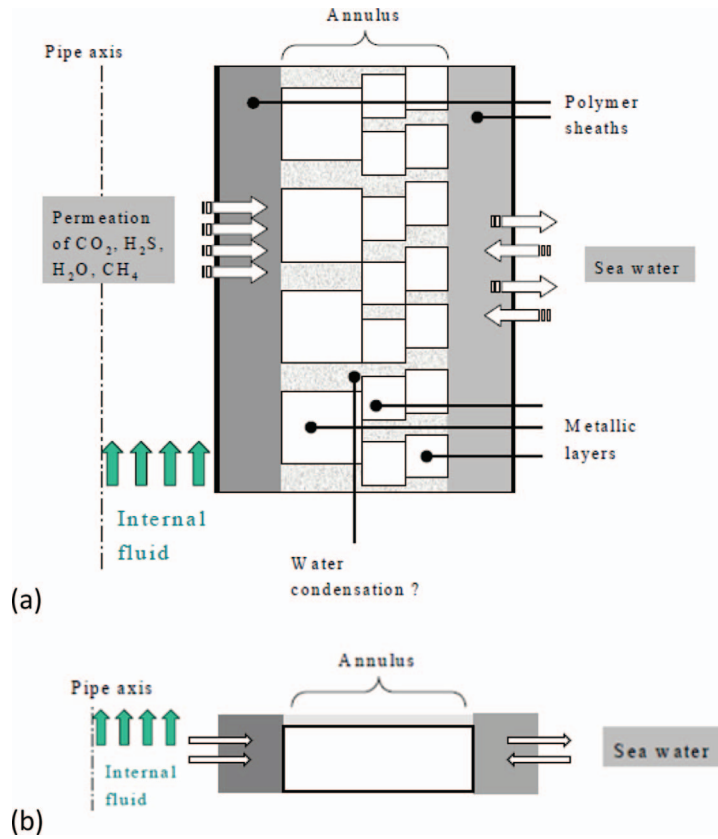


Fig. 7. (a) Complete 2D axisymmetric model with rings, (b) simplified 2D axisymmetric model.

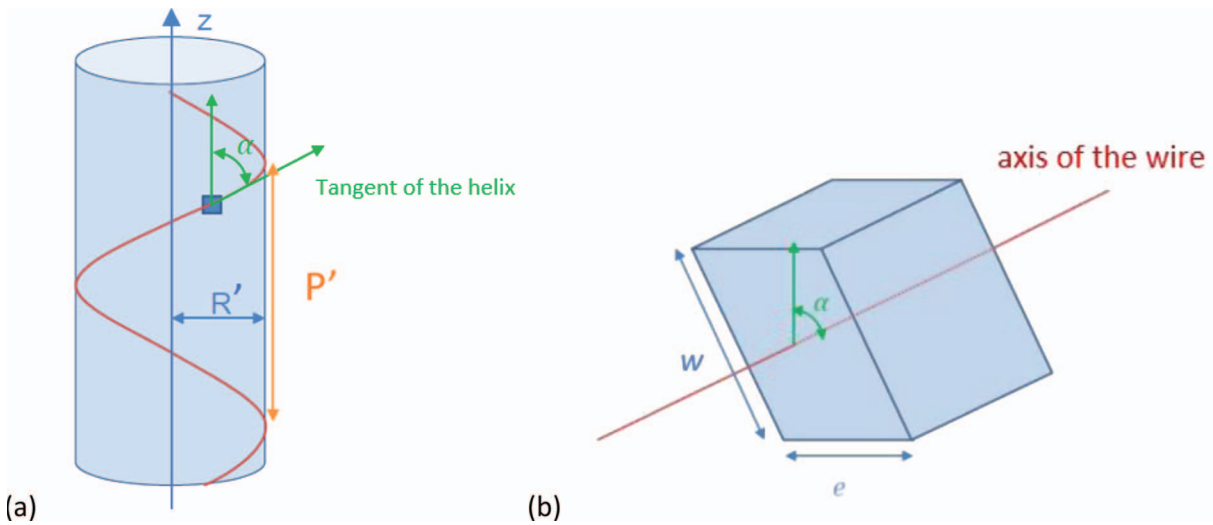
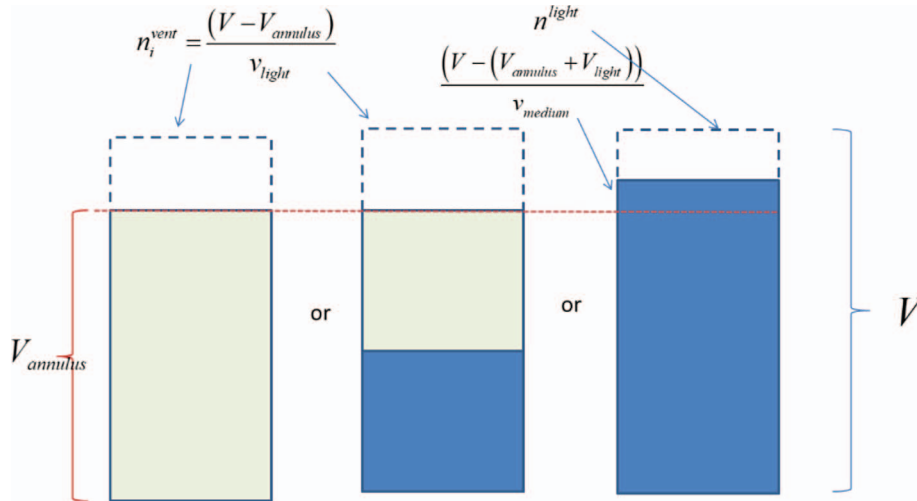


Fig. 8. Parameters of the helix (a) and parameters of the wire (b).

In case 3, the amount of light (vapour) phase is too small to reach the requested annulus volume (on the right in Fig. 9). In that case, the totality of the light phase must be removed and a part of the heavy phase. The number of moles of this extra part is its total volume,  $(V - (V_{\text{annulus}} + V_{\text{light}}))$ , divided by its molar volume,  $v_{\text{heavy}}$ , such that:

$$n_{i,t}^{\text{vent}} = n_i^{\text{light}} + \frac{(V - (V_{\text{annulus}} + V_{\text{light}}))}{v_{\text{heavy}}} x_i^{\text{heavy}}. \quad (37)$$

In a flooded annulus where the hydrostatic pressure  $P_H$  is given, the previous method is used with  $P_{\text{vent}} = P_H$  and  $\Delta P = 0$ .



**Fig. 9.** Three possibilities for venting.  $V$  is the total volume computed from the PT flash, where  $P = P_{vent\_closure}$  (which is lower than the pressure obtained from the TV flash) and  $V_{annulus}$  is the given annulus volume.

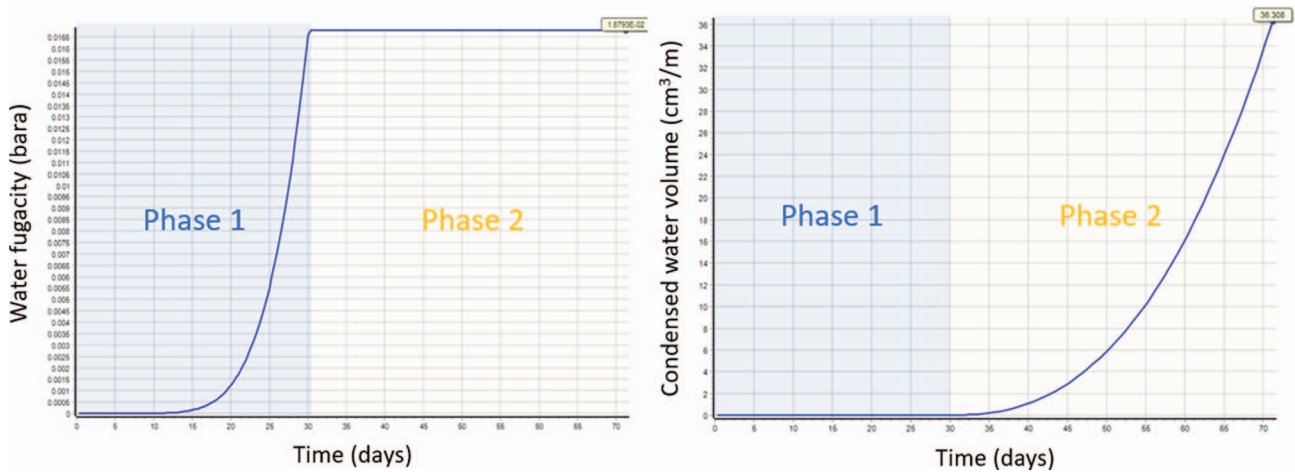


**Fig. 10.** Evolution of water fugacity and condensed water volume with time in a flexible pipe annulus in which condensation takes place.

#### 4.5 Predictions using MOLDI<sup>TM</sup> with the simplified 2D geometry

##### 4.5.1 Prediction of the condensation

Transported fluids often contain water which can permeate through the pressure sheath. Depending on the operating conditions, water condensation may occur at the coldest point of the annulus first. As MOLDI<sup>TM</sup> integrates a thermodynamic module, the software is able to predict the water condensation and the volume of water filling the annulus.

An example is presented in Figure 10: when the flexible pipe is in operation with water in the bore, in the annulus, the water fugacity increases (Phase 1). Once the saturated vapour pressure is reached, water starts condensing (Phase

2). MOLDI<sup>TM</sup> enables predicting the evolution of the water volume with time.

##### 4.5.2 Prediction of annulus venting

As explained before, annulus venting occurs when the annulus pressure is above the venting pressure.

The example of a gas injection flexible pipe equipped of a gas release valve with a venting pressure of 20 bar is presented in Figure 11: When the flexible pipe is in operation with CO<sub>2</sub> and CH<sub>4</sub> in the bore, the pressure in the annulus starts to increase due to the diffusion process (Phase 1). Once the venting pressure is reached (20 bar), the gas release valve opens and purges the excess of gases as discussed in Section 4.4. It can be observed in Figure 11 that

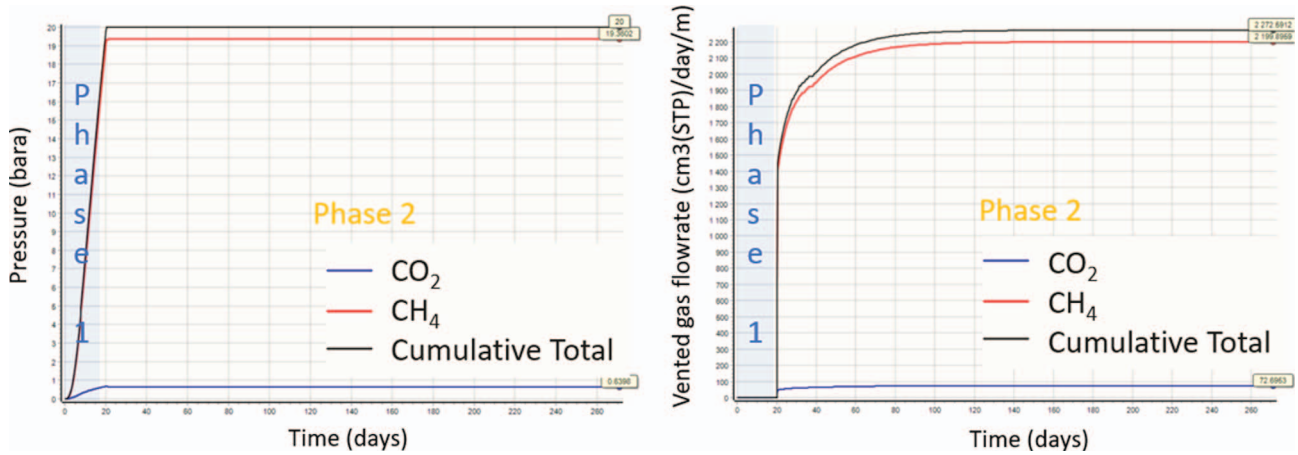


**Fig. 11.** Evolution of the pressure in the annulus of a gas injection flexible pipe with a maximum pressure of 20 bar and evolution of the vented gas flowrate with time.

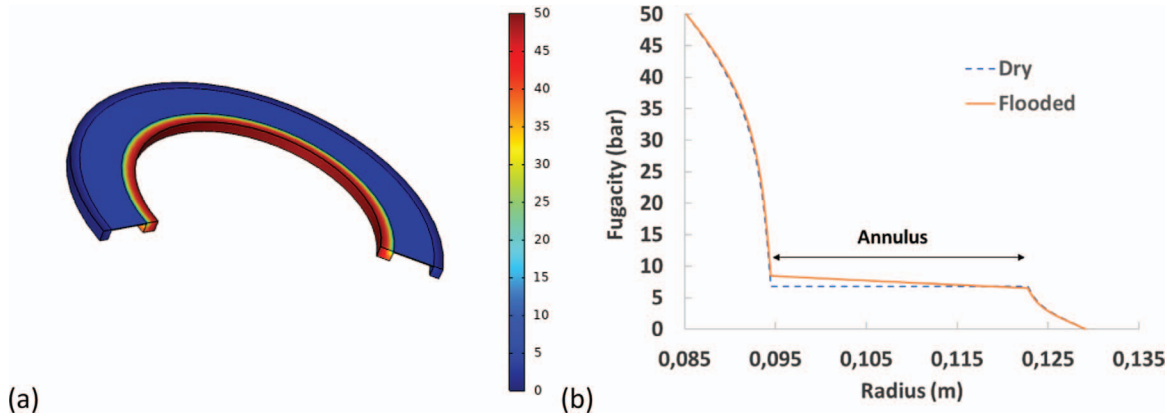


**Fig. 12.** Fugacity of CO<sub>2</sub> predicted with the 2D axisymmetric geometry for flexible F1 with a dry steel annulus (a); Comparison of fugacity gradients obtained in dry or flooded condition (b).

the vented gas flowrate starts to increase until a plateau corresponding to the steady state vented gas flowrate.

**4.5.3 Predictions of condensation and impact of flooding in the steel annulus**

To obtain accurate predictions, the flexible pipe operating conditions must be considered: the annulus containing the steel wires can be either dry, flooded by seawater or filled by condensed water coming from the bore.

As a first stage, the impact of water in the annuli can be highlighted using MOLDI™ with the simplified 2D geometry. A typical structure F1 is considered as an example; this structure is composed of a pressure sheath, a pressure vault composed of a shaped wire (zeta) and a flat wire laid with opposite angles close to -90°/+90°, a pair of armors flat wires laid with angles -35° and 35°, an external sheath. The results obtained with the 2D axisymmetric geometry, with a fugacity of CO<sub>2</sub> ( $f_{CO_2}$ ) of 50 bar in the bore, are illustrated in Figure 12:

- In the absence of water (dry conditions), a gradient of  $f_{CO_2}$  can be observed in the pressure sheath but the annulus is homogeneous.  $f_{CO_2}$  is equal to 6.8 bar at all points of the annulus.
- With water in the annulus (flooded conditions), similarly, a gradient is observed in the pressure sheath but in the annulus as well. The maximum  $f_{CO_2}$  in the annulus is 8.5 bar at the location of the inner surface of the pressure vault and the minimum  $f_{CO_2}$  is 6.6 bar below the external sheath.

Based on these first calculations, one can note that in flooded conditions, the diffusion process through the annulus is the main limiting step that governs the annulus equilibrium. An increase of 25% for  $f_{CO_2}$  at the location of the pressure vault is observed. Such increase can have a significant impact on the flexible pipe design.

When the mass transport in the annulus is a primary parameter, it is important to take into account the actual geometry of the diffusion path inside the annulus. A specific

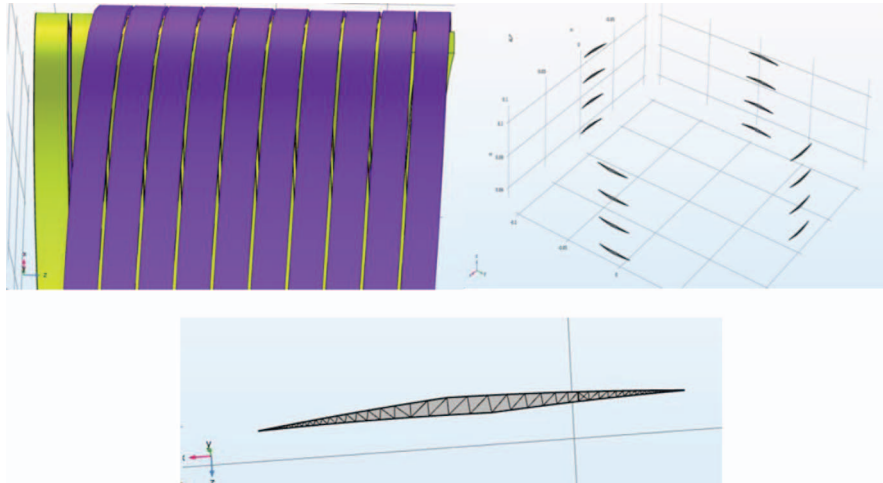


**Fig. 13.** (a) 3D representation of the zeta (yellow) and the spiral (purple); (b) Diffusion surfaces at the interface Zeta/Spiral on a whole diameter; (c) Detail of a diffusion surface pattern.

model, called 3DIFF, has thus been developed as an R&D tool to improve the predictions in flooded conditions. This model is presented in the following chapter.

## 5 Detailed 3D modeling with tortuosity in the annulus (3DIFF)

A second tool has been developed, using the same physics as described in Section 3, excluding for the time being the coupling with the thermodynamic module. Its purpose was to evaluate the effect of tortuosity on the permeation phenomenon. This tool was called 3DIFF.

### 5.1 Notion of tortuosity

Contrasting with the case of a dry annulus in which the transport mechanism of gas is very fast and leads to a homogeneous annulus, in a flooded annulus the transport mechanism is much slower, due to the presence of liquid water, and will strongly depend on the conformation of channels that are created by the steel wires (Zeta, spiral if any and armors) inside the annulus. Length, section and connectivity of all these flooded channels will create a 3D network that is needed to be considered to predict as best as possible the fugacity gradient in the structure.

To illustrate this tortuosity, we can consider for instance two steel layers in 3 dimensions: the pressure vault composed of a shaped wire (zeta) and a flat wire (spiral). In a flexible structure, these layers are wrapped above the pressure sheath. They cross each other with an opposite angle of 87–88° from the flexible pipe axis. Considering that these two wires are flat (to simplify the example), perfectly contiguous and flooded by water, it can be observed that the transport in the water contained in these layers is very limited (Fig. 13):

- Inside the zeta layer, the gas must diffuse inside the water located between each steel wire. Depending on the position of the free surface between the zeta and



**Fig. 14.** Interlocked shaped wires (zeta).

the spiral (diffusion windows), the length to go for the gas can be important. In this case, for a molecule that comes out from the pressure sheath at mid-distance of two diffusion windows, the length to go will be  $r*\pi/4$ .

- At the zeta-spiral interface, only few diffusion windows make it possible for the gas to diffuse from the Zeta to the Spiral. In this particular case, the diffusion windows are diamond-shape, and there are only 4 windows in a circumference for the species to exit. Moreover, their surface is very small.

The example shown in Figure 13 is a good illustration of the tortuosity that is created by steel wires in the annulus. Armors will create other tortuosity patterns and diffusion windows. Nevertheless, as the armors are laid with a lower angle than the pressure vault wires, the number of diffusion windows is greatly increased.

The shape of wires can also – and sometimes even more – limit the diffusion. It is specifically the case for interlocked pressure armor shaped wires, like for instance zeta wires, but applies to all typical shaped wires used as pressure armor in flexible pipe and presented in API 17B Figure 7 (Z-Shape, C-Shape, T-Shape). The resulting pattern for water diffusion between zeta wires is a kind of “Z” with two restrictions along the diffusion path (Fig. 14). The width of these restrictions has a huge influence on fugacity inside the structure.

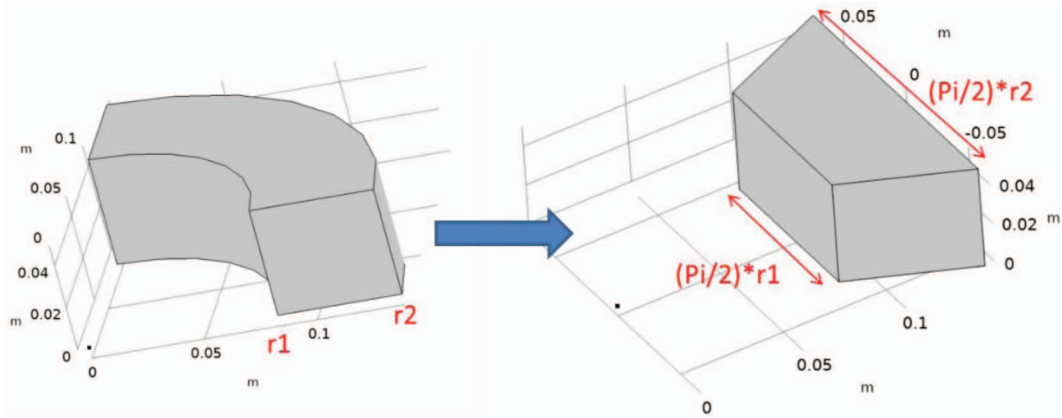


**Fig. 15.** Adaptation of the geometry to respect the increase in the diffusion surface along the radius of a pipe (as in a 2D-axisymmetrical geometry).

More generally, the presence of radial gaps between two consecutive layers can also influence fugacity gradient. For instance, a radial gap between the pressure sheath and the zeta layer can increase the species flowrate and the fugacity level at the entrance of the zeta since the diffusion surface is increased. Alternatively, radial gaps between the armors can lower the fugacity gradient inside the annulus by promoting diffusion between each layer. The final fugacity gradient will depend on all this assembly: layers, tortuosity, gaps.

## 5.2 3DIFF geometry

### 5.2.1 Description of the geometry

The first option could have been to use a 2D-axisymmetric geometry, like in MOLDI™. The mesh would have been light and the computation fast. But, considering the 3D connectivity and the fact that the wire gaps of a given layer are not aligned with the wire gaps of another layer, led to the conclusion that the 2D-axisymmetric level does not suit the needs.

The second option could have been to use a full 3D helical geometry to be fully representative. This could have been a good option to describe as best as possible the water network inside the annulus and both the helical and radial gaps between wires. Nevertheless, the full 3D helical geometry is complex. The geometry is fine with some details as small as  $10 \mu$  or even lower to describe the water network in the annulus, over several decimeters of longitudinal length in order to have a representative pattern along the flexible pipe. This need leads to heavy meshes in 3D with lots of convergence issues during meshing or resolution. Moreover, the computation time is very long (several days) even for simple structures.

An intermediate solution has been found between the 2D-axisymmetric and the 3D helical geometry. Considering that the cylindrical shape of the flexible is not essential from a diffusion point of view as long as dimensions and surface diffusion are respected, a “plane-3D” geometry was built. This is a 3-dimensions geometry in which an angular portion of the flexible pipe is straightened to represent each

layer by plane-3D elements (mainly rectangular parallelepipeds). Laying angles, thicknesses of wires and gaps between layers are the actual ones of the flexible pipe. For diffusion consideration, the 3D plane geometry is built to exhibit an increasing diffusion surface along the radius of the pipe in order to mimic the increasing diffusion surface of a 3D cylindrical geometry (Fig. 15). By this way, the diffusion surface of any layer is always equivalent to the 3D one (Fig. 16). The validation of this geometry on some cases is proposed in the next part.

### 5.2.2 Validation of the geometry

The concept of a plane 3D geometry has been validated through comparisons with helical-3D models. Using both geometries, the two values that were compared were the highest fugacity in the annulus and the steady state flow rate through the structure. As an example, one of the simplified structures that was used for this validation had the following characteristics:

- A pressure sheath and an external sheath (10 mm thickness for both).
- Internal radius: 85 mm.
- Simplified Pressure armor with two layers (Fig. 17): these wires were considered to have a rectangular section. Their laying angle was close to  $\pm 87^\circ$ , as in the flexible pipe. The gap between the wires was 1 mm.
- A thermal gradient was set between the bore ( $90^\circ\text{C}$ ) and the external medium ( $4^\circ\text{C}$ ).
- A fugacity of 100 bar of  $\text{CO}_2$  was set inside the bore for benchmark purpose.

The results obtained with both the helical 3D and the plane 3D models are presented in Table 3 considering either a dry or a flooded annulus. In both cases the models are in good agreement validating the concept of the plane 3D model.

The major advantage of the plane 3D model is its simplicity enabling to adapt its geometry to each flexible pipe characteristics and to run calculations in a reasonable time.

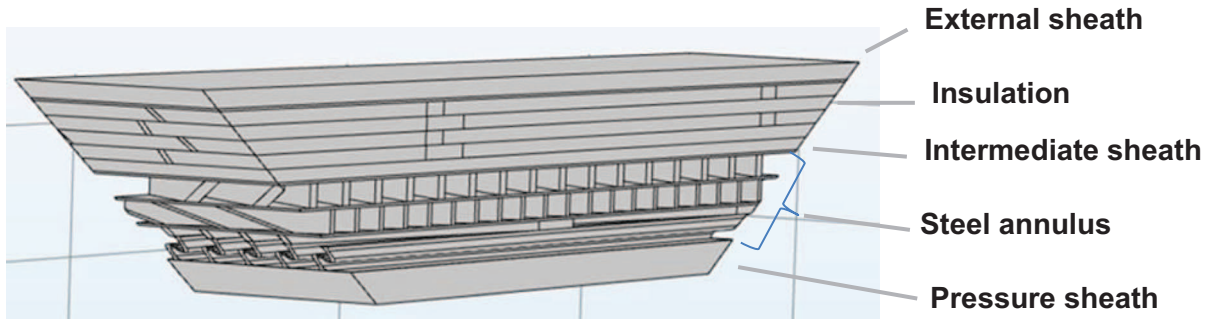


Fig. 16. Example of plane-3D geometry generated in 3DIFF.

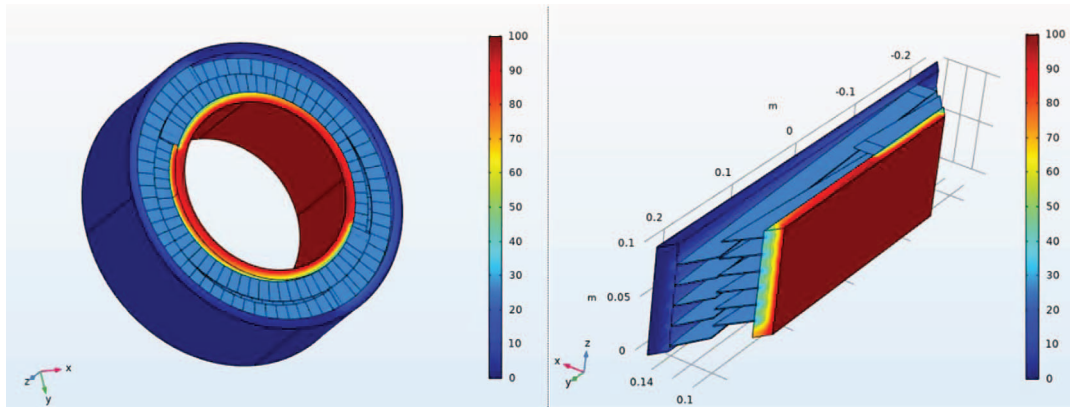


Fig. 17. Simplified structure used for the validation of 3DIFF geometry.

**Table 3.** Comparative results for Helical-3D and plane-3D geometries (simplified structure with a dry or a flooded annulus).

Annulus condition	Geometry	Highest fugacity in the annulus (bar)	Outflow rate ( $\times 10^{-9}$ mol m $^{-2}$ s $^{-1}$ )
Dry annulus	Helical 3D	27.1	1582
	Plane 3D	26.5	1638
Flooded annulus	Helical 3D	85	556
	Plane 3D	86	599

The mass transport law that is described in Section 3.1 is also applicable to 3DIFF model.

The permeability database with the physical parameters in polymers is the same as in MOLDI<sup>TM</sup> (Sect. 3.2).

### 5.3 Predictions using 3DIFF

#### 5.3.1 Calculations with dry annulus and impact of flooding

To compare with MOLDI<sup>TM</sup> predictions, 3DIFF was used to predict the steady state regime for structure F1. Figure 18 illustrates the results obtained with a fugacity of CO<sub>2</sub> of 50 bar in the bore.

In dry conditions (a), the annulus is homogeneous and the predicted  $f_{\text{CO}_2}$  is 7.3 bar. This result is well in line with MOLDI<sup>TM</sup> predictions using the simplified 2D geometry

(6.8 bar, see Sect. 4.5). When the annulus is dry, the annulus equilibrium is driven by the polymer sheaths permeability and the surface of exchange at the entry (pressure sheath) and at the exit (external sheath) of the annulus. The diffusion through the annulus free space is fast resulting in a homogeneous repartition of CO<sub>2</sub>. In such conditions, the geometry of the annulus free space does not have a significant impact; consequently both models give similar predictions.

In flooded conditions (b),  $f_{\text{CO}_2}$  varies significantly depending on the location inside the annulus. Consequently, each layer of the flexible pipe is in contact with different media. The maximum  $f_{\text{CO}_2}$  value for each layer is plotted in Figure 19 and compared to  $f_{\text{CO}_2}$  in dry conditions. The presence of water in the annulus induces an increase of  $f_{\text{CO}_2}$  by a factor up to 3.9 for the zeta and up to 2.7 for the armors. It can also be noticed that  $f_{\text{CO}_2}$  below

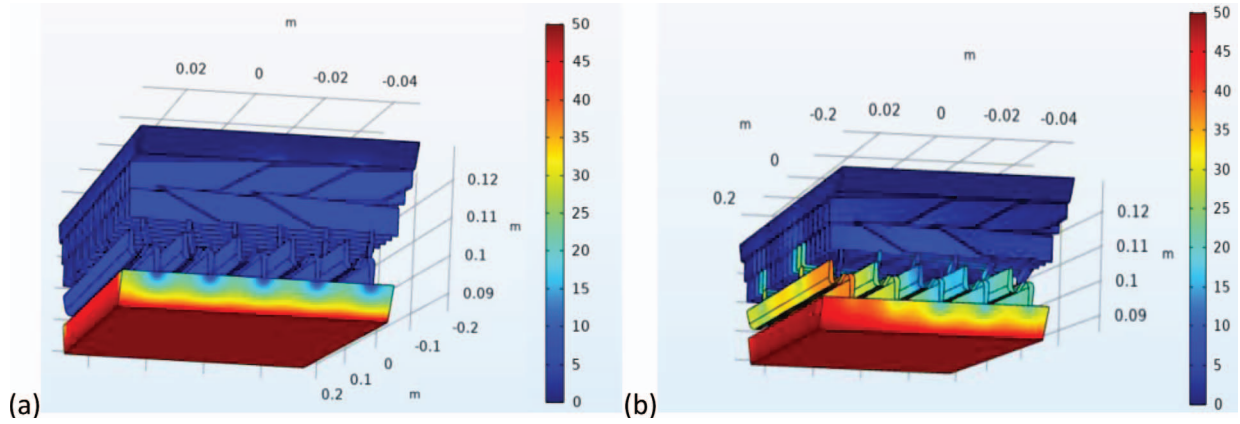


Fig. 18. Illustration of the calculation results obtained with 3DIFF software for flexible F1 with  $f_{CO_2}$  equal to 50 bar in the bore (a) with a dry steel annulus and (b) with a flooded steel annulus.

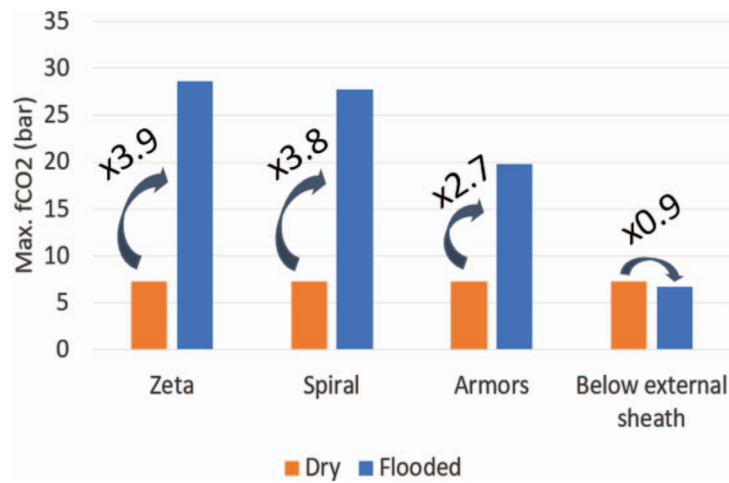


Fig. 19. Maximum  $f_{CO_2}$  values for each layer in dry and flooded conditions for the case F1 with 50 bar  $CO_2$  in the bore.

the external sheath is close to the value predicted in dry conditions. In flooded conditions, the diffusion through the annulus free space is one of the limiting process that controls  $f_{CO_2}$  in the steady state conditions.

### 5.3.2 Impact of insulation layers flooding

In 3DIFF, the geometry of the insulation layers is representative of the reality: the different layers of foam tapes are wounded around the flexible pipe. The model can thus be used to evaluate the impact of flooding in the insulation on the equilibrium in the steel annulus.

A typical insulated structure F2 is considered as an example; this structure is composed of: a pressure sheath, a pressure vault composed of a shaped wire (zeta) with a laying angle of  $87^\circ$ , a pair of armors flat wires laid with angles  $-35^\circ$  and  $35^\circ$ , an intermediate sheath, six layers of foam and an external sheath. The results obtained with 3DIFF are illustrated in Figure 20. When the insulation annulus is dry (a–b),  $f_{CO_2}$  is homogeneous in the insulation layers while when it is flooded (c–d), a gradient is observed

due to the limitation of the diffusion process by the insulation annulus. Consequently, the flooding of the insulation layers induces a global increase of  $f_{CO_2}$  in the steel annulus. The predicted  $f_{CO_2}$  for each layer is presented in Figure 21.

Similarly to the previous observations (Fig. 19), the presence of water in the steel annulus induces a significant increase in the maximum  $f_{CO_2}$  values for the zeta and the armors. This observation is valid whatever the state of the insulation annulus (in dry and flooded conditions).

The flooding of the insulation annulus has a clear negative impact on the  $CO_2$  content in contact of steel wires:

- With a dry steel annulus, the flooding of the insulation induces an increase of +57% (+3.5 bar).
- With a flooded steel annulus, the flooding of the insulation increases the maximum  $f_{CO_2}$  reported by 3DIFF. For the zeta and the armors, increases of respectively 31% (+3.4 bar) and 37% (+3.7 bar) are reported for the case F2.

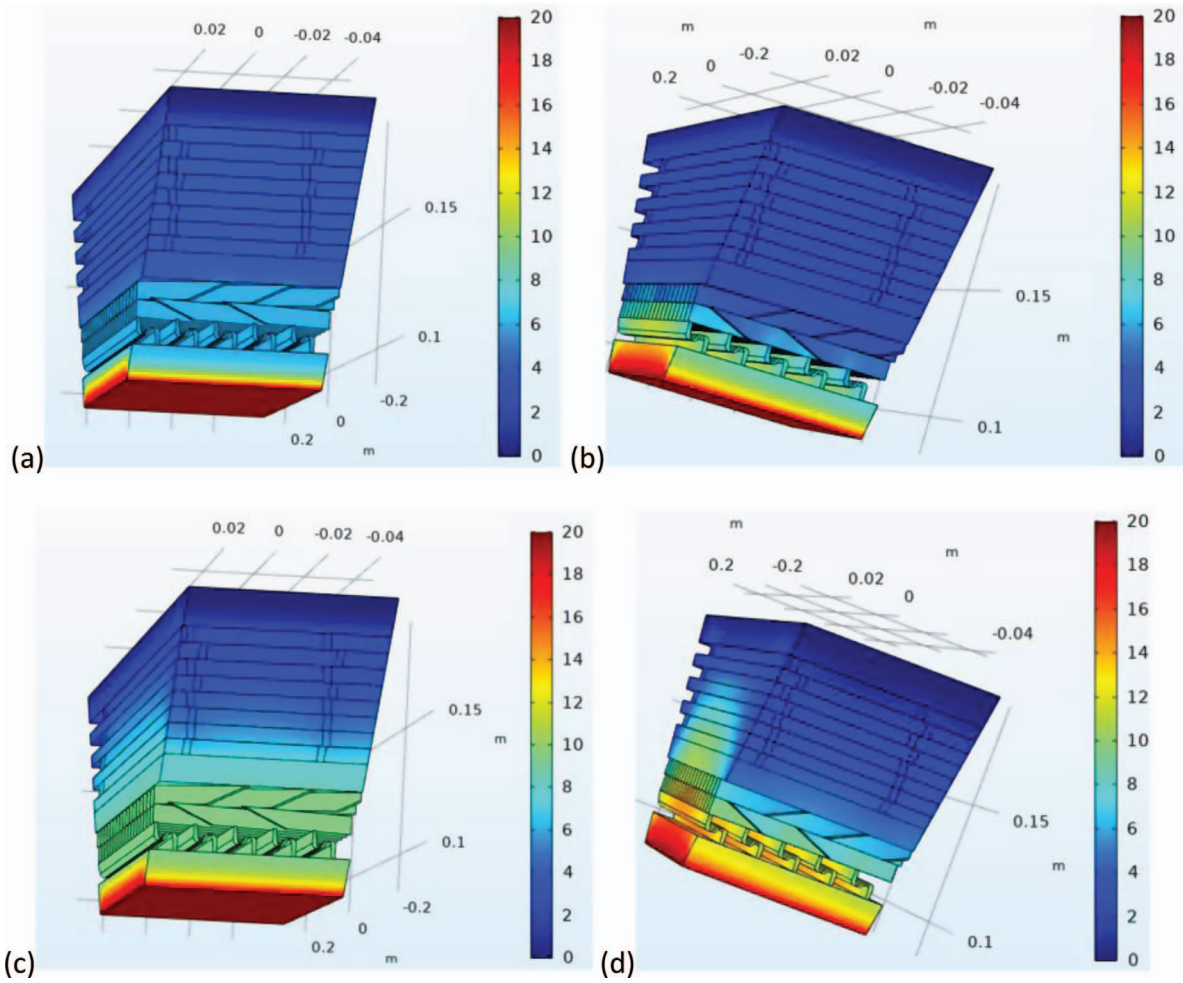


**Fig. 20.** Illustration of the calculation results obtained with 3DIFF software for flexible F2 with  $f_{CO_2}$  equal to 20 bar in the bore. (a) and (b) correspond to the dry insulation annulus, and respectively dry and flooded steel annulus. (c) and (d) correspond to the flooded insulation annulus, and respectively dry and flooded steel annulus.

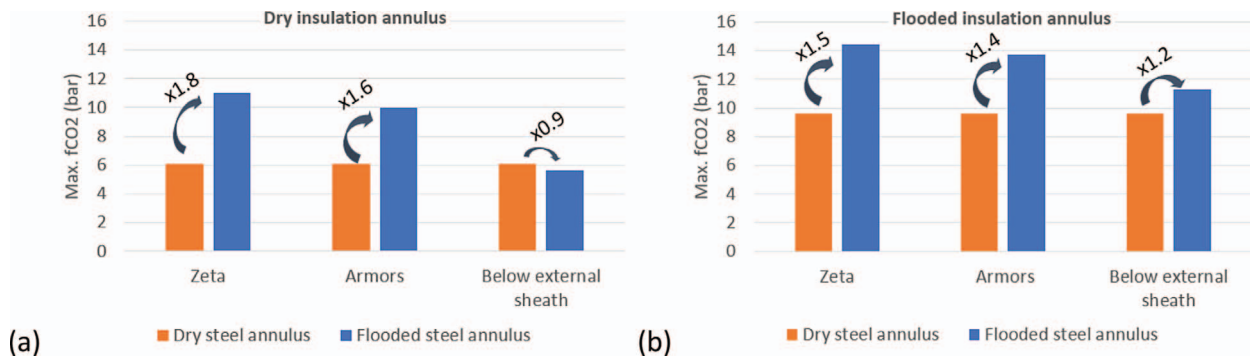


**Fig. 21.** Maximum  $f_{CO_2}$  values for each layer in dry and flooded conditions for the case F2 with 20 bar  $CO_2$  in the bore, (a) with a dry insulation annulus and (b) with a flooded insulation annulus.

Based on 3DIFF predictions, it can be concluded that the flooding of the insulation annulus is a driving parameter in the diffusion process. It is thus required to take it into account to get accurate and conservative predictions in the steel annulus.

### 5.4 Approximation method

The diffusion process through the flexible pipe structure can be seen as successive steps. Typically for a simple structure like F1: *Step 1*: diffusion through the pressure sheath; *Step 2*:

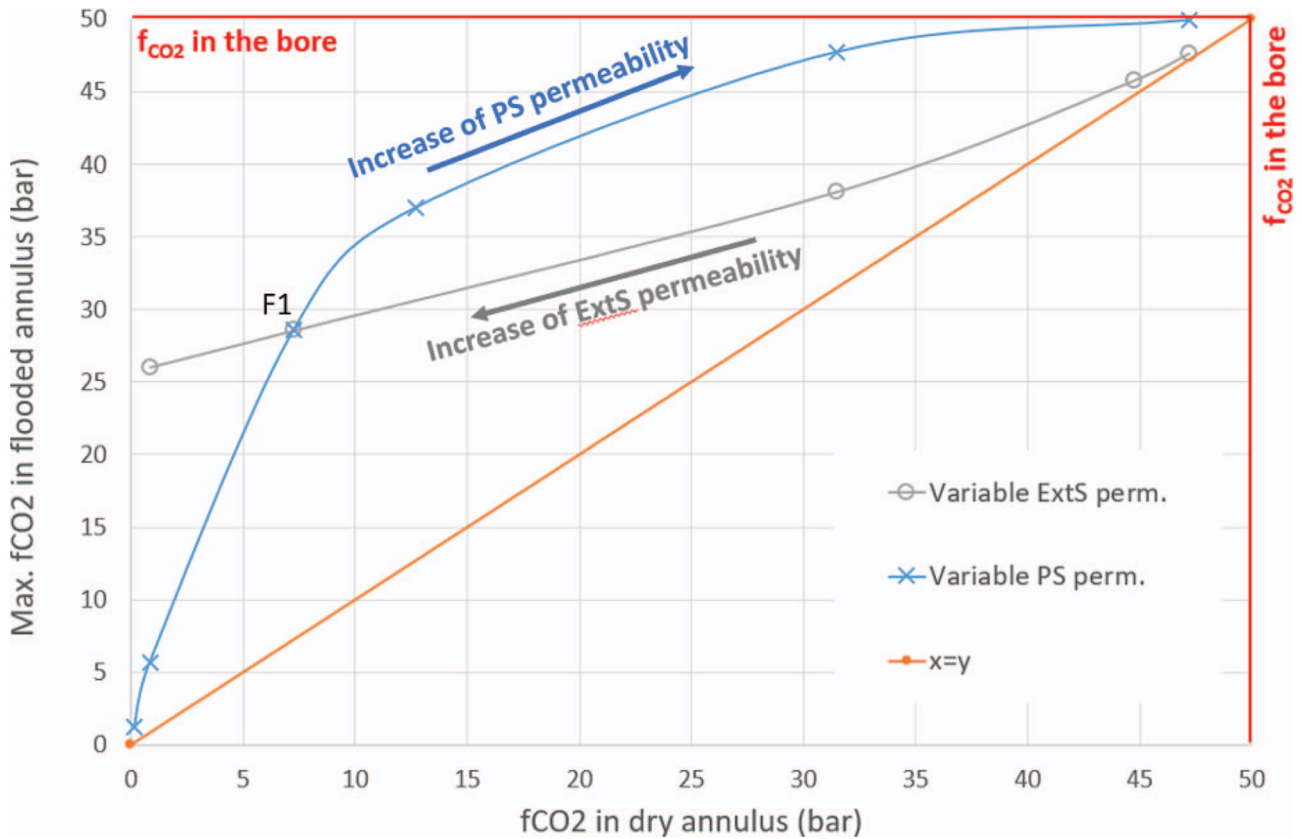


**Fig. 22.** Maximum  $f_{CO_2}$  in flooded conditions (zeta) as a function of  $f_{CO_2}$  in dry annulus with variable external sheath (ExtS) and pressure sheath (PS) permeabilities.

diffusion through the tortuous path in the annulus and *Step 3*: diffusion through the external sheath. The previous examples highlighted that *Step 2* can be the driving step. However, it is interesting to note that the weight of this step depends in fact on *Steps 1* and *3*. To illustrate this point the case F1 was slightly modified and several calculations were performed modifying the permeability of the sheaths to slow down or speed up *Steps 1* and *3*. The results are highlighted in [Figure 22](#).

Starting from F1 case, as expected, when the pressure sheath permeability is strongly increased,  $f_{CO_2}$  in the annulus tends to  $f_{CO_2}$  in the bore (50 bar in the case) and this is true in dry and flooded conditions. The same is observed when the permeability of the external sheath is strongly decreased. In such conditions, the limiting step for the diffusion is either the *Step 1* or the *Step 3*. The impact of the diffusion through the annulus free space (*Step 2*) is negligible. That is why in such cases, the predictions obtained considering a dry annulus is similar to the one obtained with a flooded annulus.

When the permeability of the pressure sheath is strongly decreased, the fugacity in the annulus tends to zero and the predictions in dry and flooded annulus are similar. In this case, the equilibrium in the annulus is clearly controlled by *Step 1*, the diffusion through the pressure sheath.

Between these two extreme situations, with a realistic case like F1, the equilibrium in the annulus is driven by the three steps and in particular the diffusion through the

tortuosity of the flooded annulus cannot be disregarded, as mentioned before. However, looking at [Figure 22](#), it is also clear that starting from F1, if we decrease the permeability of the external sheath, by changing the material for instance, the flooding impact is less and less important:  $f_{CO_2}$  in the flooded annulus becomes closer to  $f_{CO_2}$  in dry conditions.

Based on these observations, a relationship has been established between the maximum  $f_{CO_2}$  values in the flooded annulus and  $f_{CO_2}$  in dry annulus as a function of the permeability of the sheaths. This relationship is used in design to correct the value obtained with MOLDI<sup>TM</sup> with the simplified 2D axisymmetric model when it is required.

## 6 Validation

### 6.1 Validation/comparison on middle and full-scale tests results

Over the last twenty years, many medium scale and full scale tests have been performed to validate the numerical calculation of annulus composition.

Medium scale tests were performed using 4 mm-thick thermoplastic tubes. The tests set-up is illustrated in [Figure 23](#). Two steel-made half-shelves with a helical groove on the inner surface are placed around a thermoplastic tube in order to simulate the pressure vault contact on the pressure sheath of a flexible pipe. The shelves are drilled at sev-

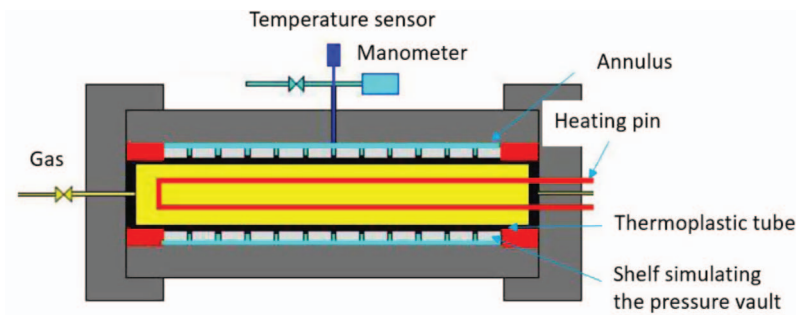


**Fig. 23.** Illustration of the medium scale tests set-up.

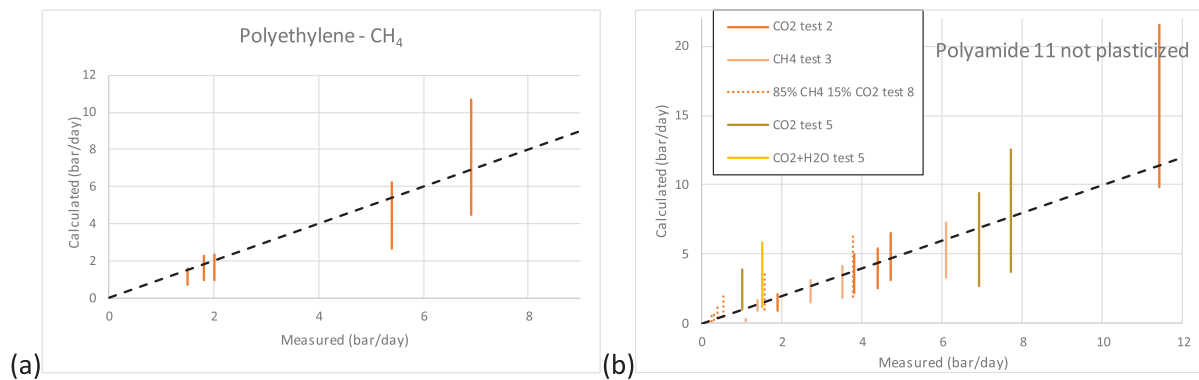


**Fig. 24.** Comparison of the calculated and the measured pressure build-up speed (a) with a polyethylene tube filled with  $\text{CH}_4$  and (b) with a polyamide 11 tube filled with either  $\text{CO}_2$ ,  $\text{CH}_4$ , a mixture of  $\text{CO}_2$  and  $\text{CH}_4$  or  $\text{CO}_2$  and water.

eral locations in order to let the gas circulate. This assembly is placed in a pressure cell (in grey). The internal volume of the tube is heated thanks to a heating pin. The annulus pressure was recorded along the test and the speed of pressure build-up was deduced from the measurements and compared to the numerical predictions. Polymer tubes made of different materials were tested with different internal pressures of pure gas, mixtures of gases or water and gas at different temperatures.

Examples of results are presented in Figure 24 with the calculated and the measured pressure build-up speed for a polyethylene tube tested with methane (a) and for a not plasticized polyamide 11 tested with either  $\text{CO}_2$ ,  $\text{CH}_4$ , a mixture of  $\text{CH}_4$  and  $\text{CO}_2$  and water and  $\text{CO}_2$  (b). This type of device does not allow to ensure the masking effect. Thus, MOLDI™ calculations have been done with and without masking, leading to vertical lines. These graphics show that the measurements are within the uncertainty of the calculations.

Twelve full scale tests have been analyzed to compare the results with MOLDI™ predictions. Since complete flexible pipe structures were tested, the tests induced many parameters which cannot be fully captured in calculations (*e.g.*, bore filling and mixing procedure which influence the fugacities calculation, external sheath diameter light variation, sheath as-built thickness, etc.). As a result, calculations cannot perfectly fit with measurements. However, as shown in Table 4, a good agreement was found between measured and calculated vented flowrates.

## 6.2 Validation/comparison with data in service

Three cases have been simulated with MOLDI™. The operating conditions and the results are presented in Table 5. For the two first cases, the annulus composition was analyzed in service and compared to the calculated composition. For the third case, the volume of condensed water in the annulus was measured during the dissection of the flexible pipe and this volume is compared to the calculated one.

In terms of composition, results are not far from the measurements if we consider the operational variability that can be encountered in service compared to the calculations performed with only one set of parameters. Looking at the third case, it can be noticed that the water condensation predictions are strongly conservative compared to the measurements.

## 6.3 Preliminary results in flooding conditions

A new permeation unit has been specifically designed to measure local concentrations of gases dissolved in water. This unit is composed of three cells separated by two polymer membranes to simulate the flexible pipe in operation: the first cell being the bore, the second one a simplified annulus and the third one the external seawater. This brand new equipment enables to have a good control of the testing parameters and an accuracy in the measurements.

**Table 4.** Example of full scale tests conditions and results (measured and calculated vented flowrate).

Structure internal diameter	9"	7"
Pressure sheath material	PVDF (3 layers)	PVDF
Bore fluids	CO <sub>2</sub> , CH <sub>4</sub> , H <sub>2</sub> O	CO <sub>2</sub>
Bore <i>P</i> (bar)	220	300
<i>T</i> (°C)	123	130
Measured vented flowrate	3.5–8.5 L/day	4.5 L/h
Calculated vented flowrate	6 L/day	6.5 L/h

**Table 5.** Real cases conditions and measurements compared to MOLDI™ results (in terms of annulus composition or condensed water dissection).

Flexible pipe type	Gas injection	Oil Production	Production
Internal diameter	8"	8"	6"
Pressure sheath material	PA	PVDF	PA
Bore <i>P</i> (bar)	380	115	386
<i>T</i> (°C)	53	103	60–75
Measured	Annulus composition: 2.1% N <sub>2</sub> , 18.7% CO <sub>2</sub> , 79.2% CH <sub>4</sub>	Annulus composition: 20.7% CO <sub>2</sub> , 79.9% CH <sub>4</sub>	Annulus condensed water from dissection: 10 L
MOLDI™	2% N <sub>2</sub> , 17.5% CO <sub>2</sub> , 79.9% CH <sub>4</sub>	25.3% CO <sub>2</sub> , 71.6% CH <sub>4</sub>	134.4 L

An extensive tests campaign is planned to fully validate the modeling predictions, in dry and flooded annulus. However, preliminary results already highlighted a gradient of dissolved CO<sub>2</sub> in the water in line with the results from the calculations. In these first tests, at the equilibrium, the concentration of CO<sub>2</sub> at the entry of the second cell can be between 5 and 10 times higher than the concentration of CO<sub>2</sub> at the exit of this cell, only due to the flooding by water. The impact of the slow diffusion in the water is thus clearly evidenced and those results match very well with 3DIFF predictions.

## 7 Discussion: application area and way forward

The impact of the annulus tortuosity in case of flooding is clearly highlighted using 3DIFF. In this model the geometry of the annulus is representative of the reality. However it does not integrate a thermodynamic module; the predictions are only based on the mass transport law. As a consequence, the actual maximum pressure in the annulus and the possible opening of a gas release valve are not taken into account. One must consider 3DIFF results with caution in order to avoid over conservatism.

Typically, when the flexible pipe operates in very deep water, allowing the gases to stay fully dissolved under the bubble point in the annulus, the results obtained with 3DIFF with a flooded annulus can be considered. On the opposite, when there is a gas phase in the annulus inducing a purge through the gas release valves, 3DIFF results can be too conservative.

MOLDI™ is the software used for flexible pipes designs to predict the annulus equilibrium. Among its characteristics, the water condensation can be predicted and the

purging through Gas Release Valve (GRV) is taken into account. This design software is efficient in terms of calculation time and it integrates a correction to take into account the effects of tortuosity and flooding when it is applicable.

3DIFF is the R&D tool that is under continuous evolution to refine the annulus medium predictions and identify the best developments for the future flexible pipes. The validation of the results obtained in flooded conditions has already started and promising results have been obtained. The test campaign is still on-going to validate the predictions in various conditions of temperature and pressure and with different materials. The impact of the geometry will be further highlighted and tests will also be performed above the saturation, with a gas phase.

The continuous improvement of the permeability database is also a major axis to refine the models predictions. As stated before, standard tests are typically performed in two compartments cell: one gas charging cell and one gas collection cell separated by a polymer membrane. New parameters are being investigated; in particular, in the recent years, the compression of the polymer has been highlighted as an important parameter. For this purpose, a specific cell has been adapted enabling to test polymer tubes at high pressure.

## 8 Conclusion

Flexible pipes material selection is equally driven by the mechanical loadings and the properties of the annulus. Having reliable annulus environment predictions is thus essential to optimize flexible pipe design and avoid product performance issues in operation.

In this paper the physical principles and the governing equations of the diffusion models developed by *IFPen* and *TechnipFMC* were detailed. A modification of Fick's law is used to describe the mass transport: the gradient of fugacity is now the driving force for the diffusion process. The thermodynamic module was improved using the CPA equation of state that is well adapted to the mixture of interest. A specific model called 3DIFF was developed in order to investigate the impact of water flooding associated with the complex geometry of a flexible pipe annulus. It was highlighted that the tortuosity and the flooding of the annulus result in a strong heterogeneity and in an increase of the annulus severity. Similarly, the flooding of the insulation annulus is a key factor that also results in an increase of severity of the medium in contact with steel wires.

MOLDI<sup>TM</sup> has been upgraded and remains the certified design software that is used by *TechnipFMC*. As with the former versions, MOLDI<sup>TM</sup> makes it possible to predict the fugacities of CO<sub>2</sub>, CH<sub>4</sub> and H<sub>2</sub>S in the annulus, the water condensation and the vented gas flowrates. A methodology has been developed to take into account the effects of tortuosity and flooding when it is applicable.

Medium scale and full scale tests together with field data were used to validate the software. Besides a specific experimental unit was developed to validate the impact of flooding. Preliminary results are positive. To go further in the validation, an experimental program is on-going; the results will be published later on.

## References

- 1 TechnipFMC website. Flexible pipes, <https://www.technipfmc.com/en/what-we-do/subsea/subsea-systems/subsea-infrastructure/flexible-pipes/>.
- 2 Specification for Unbonded Flexible Pipe (2009) *ANSI/API Specification 17J*, Third Edition.
- 3 Benjelloun-Dabaghi Z., de Hemptinne J.-C., Jarrin J., Leroy J.-M., Aubry J.-C., Saas J.N., Taravel-Condac C. (2002) MOLDI<sup>TM</sup>: A fluid Permeation model to calculate the annulus composition in flexible pipes, *Oil Gas Sci. Technol. - Rev. IFP Energies nouvelles* **57**, 2, 177–192.
- 4 Désamais N., Taravel-Condac C. (2010) A new methodology allowing the use of high strength steels with H<sub>2</sub>S in ultra deep water flexible pipe, in: *The Deep Offshore Technology International Conference and Exhibition, Amsterdam*.
- 5 Désamais N., Taravel-Condac C. (2009) On the beneficial influence of a very low supply of H<sub>2</sub>S on the hydrogen embrittlement resistance of carbon steel wires in flexible pipe annulus, in: *Offshore Technology Conference, OTC-19950-MS, Houston, Texas*.
- 6 Ke L., Taravel-Condac C., Kittel J., Mingant R., Duret-Thual C., Querez V. (2017) Optimizing the design of unbonded flexible pipelines with more realistic predictions of pH and H<sub>2</sub>S content in the annulus, in: *International Conference on Ocean, Offshore and Arctic Engineering, Trondheim, OMAE2017-61129*.
- 7 Kittel J., Grosjean F., Forot C., Désamais N., Taravel-Condac C., Duret-Thual C., Fourny P. (2013) Impact of time of exposure on HIC testing of very high strength steel in low H<sub>2</sub>S environments, in: *Eurocorr, The European Corrosion Congress, Estoril, Portugal*.
- 8 Vidigal J., Taravel-Condac C., Meira J., De La Tour P. (2017) Impact of H<sub>2</sub>S consumption and anti-H<sub>2</sub>S layer on flexible pipe design, in: *Offshore Technology Conference, OTC-27733-MS, Houston, Texas*.
- 9 Onsager L. (1931) Reciprocal relations in irreversible processes. I, *Phys. Rev.* **37**, 405.
- 10 Taylor R., Krishna R. (1993) *Multicomponent mass transfer*, John Wiley & Sons.
- 11 Mauviel G. (2003) Transport multi-composants dans les polymères: séparation hydrocarbures / hydrogène par membrane à sélectivité inverse, *Ph.D Thesis*, Lorraine University.
- 12 Flaconeche B., Martin J., Klopffer M.H. (2001) Permeability, diffusion and solubility of gases in Polyethylene, Polyamide 11 and Poly (Vinylidene Fluoride), *Oil Gas Sci. Technol. - Rev. IFP Energies nouvelles* **56**, 3, 261–278.
- 13 Chapman W.G., Gubbins K.E., Jackson G., Radosz M. (1989) SAFT: Equation-of-state solution model for associating fluids, *Fluid Phase Equilib.* **52**, 31–38.
- 14 Gross J., Sadowski G. (2001) Perturbed-chain SAFT: Equation of state based on a perturbation theory for chain molecules. *Ind. Eng. Chem. Res.* **40**, 4, 1244–1260.
- 15 Wang C., Rubin A., von Solms N. (2013) Qualification of polymer materials for high pressure CO<sub>2</sub> flexible pipe structures, in: *Society of Petroleum Engineering, Offshore Technology Conference, SPE-FOTC-24468-MS, Rio de Janeiro, Brazil*.
- 16 Kontogeorgis G., Voutsas E., Yakoumis I., Tassios D. (1996) An equation of state for associating fluids, *Ind. Eng. Chem. Res.* **35**, 111, 4310–4318.
- 17 Ruffine L. (2005) Equilibres de phases à basse température de systèmes complexes CO<sub>2</sub> – Hydrocarbures légers – méthanol – eau : mesures et modélisation, *PhD Thesis*, Lyon 1 University.
- 18 Ruffine L., Barreau A., Mougin P. (2006) How to represent hydrogen sulfide within the CPA equation of state, *Ind. Eng. Chem. Res.* **45**, 122, 7688–7699.
- 19 Tsvintzelis I., Kontogeorgis G., Michelsen M., Stenby E. (2010) Modeling phase equilibria for acid gas mixtures using the CPA equation of state. I. Mixtures with H<sub>2</sub>S, *AIChE J.* **56**, 111, 2965–2982.
- 20 Valtz A., Chapoy A., Coquelet C., Paricaud P., Richon D. (2004) Vapour-liquid equilibria in the carbon dioxide-water system, measurement and modelling from 278.2 to 318.2K, *Fluid Phase Equilib.* **226**, 333–344.
- 21 Nakayama T., Sagara H., Arai K., Saito S. (1987) High pressure liquid-liquid equilibria for the system of water, ethanol and 1,1-difluoroethane at 323.2K, *Fluid Phase Equilib.* **38**, 11–2, 109–127.
- 22 Eduardo Pereira Siqueira Campos C., Gomes D'Amato Villardi H., Luiz Pellegrini Pessoa F., Maria Cohen Uller A. (2009) Solubility of carbon dioxide in water and hexadecane: experimental measurement and thermodynamic modeling, *J. Chem. Eng. Data* **54**, 110, 2881–2886.
- 23 Vilcu R., Gainar I. (1967) Löslichkeit der Gase unter Druck in Flüssigkeiten. I. Das System Kohlendioxid-Wasser, *Rev. Roum. Chim.* **12**, 181–189.
- 24 Coan C., King A. (1971) Solubility of water in compressed carbon dioxide, nitrous oxide, and ethane. Evidence for hydration of carbon dioxide and nitrous oxide in the gas phase, *J. Am. Chem. Soc.* **93**, 1857–1862.

- 25 Hou S.-X., Maitland G., Trusler J. (2013) Measurement and modeling of the phase behavior of the (carbon dioxide + water) mixture at temperatures from 298.15 K to 448.15 K, *J. Supercrit. Fluids* **73**, 87–96.
- 26 Wiebe R., Gaddy V. (1941) Vapor phase composition of carbon dioxide-water mixtures at various temperatures and at pressures to 700 atmospheres, *J. Am. Chem. Soc.* **63**, 12, 475–477.
- 27 Serpa F.S., Vidal R.S., Amaral-Filho J.H.B., do Nascimento J.F., Ciambelli J.R.P., Figueiredo C.M.S., Salazar-Banda G. R., Santos A.F., Fortuny M., Franceschi E., Dariva C. (2013) Solubility of carbon dioxide in ethane-1,2-diol-water mixtures, *J. Chem. Eng. Data* **58**, 112, 3464–3469.
- 28 Dalmolin I., Skovroinski E., Biasi A., Corazza C., Dariva C., Oliveira J. (2006) Solubility of carbon dioxide in binary and ternary mixtures with ethanol and water, *Fluid Phase Equilib.* **245**, 12, 193–200.
- 29 Kiepe J., Horstmann S., Fischer K., Gmehling J. (2003) Experimental determination and prediction of gas solubility data for methane + water solutions containing different monovalent electrolytes, *Ind. Eng. Chem. Res.* **42**, 121, 5392–5398.